The American Journal of Pathology, Vol. 175, No. 6, December 2009

DOI: 10.2353/ajpath.2009.081096

Neurobiology

Increased Activity and Altered Subcellular Distribution of Lysosomal Enzymes Determine Neuronal Vulnerability in Niemann-Pick Type C1-Deficient Mice

Asha Amritraj,* Kyle Peake,† Anitha Kodam,* Chiara Salio,‡ Adalberto Merighi,‡ Jean E. Vance,† and Satyabrata Kar*†

From the Departments of Psychiatry and Medicine,† Centre for Prions and Protein Folding Diseases, University of Alberta, Edmonton, Alberta, Canada; and Department of Veterinary Morphophysiology,‡ University of Turin, Grugliasco, Italy*

Niemann-Pick disease type C (NPC), caused by mutations in the *Npc1* or *Npc2* genes, is a progressive neurodegenerative disorder characterized by intracellular accumulation/redistribution of cholesterol in a number of tissues including the brain. This is accompanied by a severe loss of neurons in selected brain regions. In this study, we evaluated the role of lysosomal enzymes, cathepsins B and D, in determining neuronal vulnerability in NPC1-deficient (*Npc1*$^{-/-}$) mouse brains. Our results showed that *Npc1*$^{-/-}$ mice exhibit an age-dependent degeneration of neurons in the cerebellum but not in the hippocampus. The cellular level/expression and activity of cathepsins B and D are increased more predominantly in the cerebellum than in the hippocampus of *Npc1*$^{-/-}$ mice. In addition, the cytosolic levels of cathepsins, cytochrome *c*, and Bax2 are higher in the cerebellum than in the hippocampus of *Npc1*$^{-/-}$ mice, suggesting a role for these enzymes in the degeneration of neurons. This suggestion is supported by our observation that degeneration of cultured cortical neurons treated with U18666A, which induces an NPC1-like phenotype at the cellular level, can be attenuated by inhibition of cathepsin B or D enzyme activity. These results suggest that the increased level/activity and altered subcellular distribution of cathepsins may be associated with the underlying cause of neuronal vulnerability in *Npc1*$^{-/-}$ brains. Therefore, their inhibitors may have therapeutic potential in attenuating NPC pathology. *(Am J Pathol 2009, 175:2540–2556; DOI: 10.2353/ajpath.2009.081096)*

Niemann-Pick disease type C (NPC) is an autosomal recessive neurovisceral disorder caused by mutations in the *Npc1* or *Npc2* gene. NPC1 is a membrane protein that contains a sterol-sensing domain and resides primarily in late endosomes/lysosomes, whereas NPC2 is a soluble protein that resides primarily in lysosomes.[1–4] The loss of function of either protein results in intracellular accumulation of unesterified cholesterol and glycosphingolipids within the endosomal-lysosomal (EL) system in a number of tissues including the brain. In addition, there is evidence that homeostatic responses to exogenously supplied cholesterol and activation of cholesterol esterification are severely impaired in cells lacking functional NPC1. These defects in cholesterol accumulation/homeostasis trigger abnormal liver and spleen function as well as widespread neurological deficits including ataxia, dystonia, seizures, and dementia that eventually lead to premature death.[5–9] Interestingly, BALB/cNctr-*Npc*$^{N/N}$ mice, which do not express NPC1 protein because of a spontaneous deletion/insertion mutation in the *Npc1* gene, have been shown to recapitulate pathological features associated with NPC disease. These *Npc1*$^{-/-}$ mice are asymptomatic at birth but gradually develop tremor and ataxia, dying prematurely at ~3 months.[10–13] As in the human disease, *Npc1*$^{-/-}$ mice show accumulation of unesterified cholesterol in the EL system and exhibit ac-

Supported by grants from the Canadian Institutes of Health Research (S.K. and J.E.V.) and the Ara Parseghian Medical Research Foundation (J.E.V.). K.P. is a recipient of studentship awards from the Alberta Heritage Foundation for Medical Research (AHFMR) and Natural Sciences and Engineering Research Council of Canada. S.K. is a recipient of Canada Research Chair (Tier-II) in Neurodegenerative Diseases and a Senior Scholar award from the AHFMR.

Accepted for publication August 12, 2009.

Supplemental material for this article can be found on *http://ajp.amjpathol.org*.

Address reprint requests to Satyabrata Kar, Ph.D., Centre for Prions and Protein Folding Diseases, Departments of Medicine (Neurology) and Psychiatry, University of Alberta, Edmonton, AB, Canada T6G 2M8. E-mail: skar@ualberta.ca.

tivation of microglia and astrocytes as well as degradation of the myelin sheath throughout the central nervous system. Progressive loss of neurons is particularly evident in the prefrontal cortex, thalamus, brainstem, and cerebellum but not in the hippocampal formation.[13–18] However, at present, very little is known about the underlying mechanisms associated with the vulnerability of select populations of neurons in *Npc1*$^{-/-}$ mice.

A number of earlier studies have shown that the EL system, the major site of cholesterol accumulation in NPC pathology, consists of two dynamic interrelated cellular pathways: the endocytic pathway and the lysosomal system. Under normal conditions, the EL system serves as an important site for intracellular protein turnover and proteolytic processing of certain proteins mediated by lysosomal hydrolases termed cathepsins.[19–21] After their synthesis in the endoplasmic reticulum, cathepsins bind to the insulin-like growth factor-II (IGF-II)/mannose 6-phosphate (M6P) receptor on the trans face of the Golgi complex and are transported in vesicles to the EL system.[22–24] The importance of lysosomal enzymes in the proper functioning of the EL system is underscored by the fact that altered synthesis, sorting, or targeting of lysosomal enzymes is the molecular basis of more than 40 inherited disorders associated with extensive neurodegeneration, mental retardation and often progressive cognitive decline.[19,25–27]

There is evidence that increased endosome volumes and/or levels of cathepsins, such as cathepsins B and D, can mediate cell death by inducing lysosomal destabilization and enzyme leakage into cell cytosol, as is observed during oxidative stress[28] and experimental brain ischemia in primates.[29] Conversely, a number of recent studies have shown that lysosomal enzyme expression/levels can be up-regulated in the absence of cell death as a compensatory mechanism to repair damage/injury.[30–33] Thus, it seems that lysosomal enzymes are not only involved in the degeneration of neurons but also in the protection of neurons against toxicity in a variety of experimental as well as pathological paradigms. Although the EL system, the major site of cholesterol accumulation in NPC1-deficient cells, has been suggested to play a critical role in the development of NPC pathology,[6–8] very little is known about the significance of lysosomal cathepsins in determining neuronal vulnerability associated with the disease. To address this issue, we measured age-related changes in the levels, distribution, and activity of cathepsins B and D in the hippocampus and cerebellum of *Npc1*$^{-/-}$ and age-matched control mice. In parallel, we evaluated the levels and distribution of the IGF-II/M6P receptor in *Npc1*$^{-/-}$ and control mice to establish whether factors regulating cathepsin bioavailability can also influence the development of pathological changes. In addition, using cultured mouse cortical neurons we determined the significance of cathepsins B and D in the degeneration of neurons after accumulation of cholesterol. Our results reveal that alterations in the levels/activity as well as subcellular distribution of the lysosomal enzymes may be one of the underlying mechanisms associated with the selective neuronal vulnerability observed in NPC pathology.

Materials and Methods

Materials

Polyacrylamide electrophoresis gels (4 to 20%) and cell culture reagents such as Hanks' balanced salt solution, fetal bovine serum, Neurobasal media, B27, N2, and trypsin were purchased from Invitrogen (Burlington, ON, Canada), and the enhanced chemiluminescence (ECL) kit was obtained from Amersham (Mississauga, ON, Canada). Fluoro-Jade C was purchased from Histochem (Jefferson, AR) and the Qproteome Cell Compartment kit was from QIAGEN Inc. (Mississauga, ON, Canada). The cathepsin B assay kit and its inhibitor CA-074 methyl ester were obtained from Calbiochem (San Diego, CA), and the cathepsin D assay kit, pepstatin A, lysosomal isolation kit, and fluorescein isothiocyanate (FITC)-tagged lectin were purchased from Sigma (Oakville, ON, Canada). The class II amphiphilic drug U18666A was purchased from Biomol Research Laboratories (Plymouth, PA). Two different polyclonal IGF-II/M6P receptor antisera used in this study were obtained as generous gifts from Dr. C. D. Scott (Kolling Institute of Medical Research, St. Leonards, Australia) and Dr. R. G. MacDonald (University of Nebraska Medical Center, Omaha, NE). The characterization and specificity of these two antisera have been described previously.[34,35] Polyclonal anti-cathepsin B, anti-lysosomal associated membrane protein 2, anti-cathepsin D, anti-Bax2, anti-N cadherin, anti-histone, anti-beclin-1, anti-myelin associated glycoprotein, and anti-apoptosis-inducing factor (AIF) were obtained from Santa Cruz Biotechnology (San Diego, CA). Polyclonal anti-ionizing calcium-binding adaptor molecule 1 (Iba1) was purchased from Wako Chemicals (Richmond, VA), and anti-glial fibrillary acidic protein (GFAP), anti-glyceraldehyde-3-phosphate dehydrogenase, anti-calbindin, anti-β-actin, and filipin were from Sigma. Polyclonal anti-cleaved caspase-3 was from Cell Signaling (Beverly, MA), neuron-specific marker NeuroTrace was from Invitrogen, anti-microtubule-associated protein1 light chain 3 (LC3), and anti-cytochrome *c* were from BD Biosciences (Mississauga, ON, Canada). Secondary antisera such as donkey anti-goat Texas Red, anti-rabbit FITC, and anti-mouse FITC were from Jackson ImmunoResearch Laboratories (West Grove, PA). All other chemicals were from either Sigma or Fisher Scientific (Whitby, ON, Canada).

Npc1$^{-/-}$ and Control Mice

The age-matched control and *Npc1*$^{-/-}$ mice were obtained from a breeding colony of BALB/cNctr-*Npc*$^{N/+}$ mice established at the University of Alberta after the original breeding pairs were purchased from The Jackson Laboratory (Bar Harbor, ME). The mice were maintained under temperature-controlled conditions with a 12-hour light, 12-hour dark cycle according to institutional guidelines and were supplied with food and water *ad libitum*. Because *Npc1*$^{-/-}$ mice do not produce offspring, *Npc1* heterozygous (*Npc1*$^{+/-}$) mice were used to generate *Npc1*$^{-/-}$ and controls (*Npc1*$^{+/+}$). The *Npc1*

genotype was determined from tail clippings by PCR analysis of genomic DNA.[11] *Npc1*$^{-/-}$ and control mice from three different age groups (4, 7, and 10 weeks old) were sacrificed by decapitation, their brains were rapidly removed, and areas of interest (prefrontal/frontal cortex, hippocampus, and cerebellum) were dissected and frozen immediately in dry ice for biochemical assays. For light microscopic histological studies, *Npc1*$^{-/-}$ and control mice (4, 7, and 10 weeks old) were anesthetized with 4% chloral hydrate and then perfused intracardially with PBS (0.01 M, pH 7.4), followed by 4% paraformaldehyde or Bouin's solution. Brains were sectioned (20 or 40 μm) on a cryostat and collected in a free-floating manner for further processing. For electron microscopic studies, 4 week-old control and *Npc1*$^{-/-}$ mice (two animals per group) were perfused with PBS, followed by 4% paraformaldehyde and 2% glutaraldehyde solution. The brains were then postfixed with the same fixative for 4 hours at 4°C, washed in PBS, and processed for electron microscopy.

Mouse Cortical Neuron Cultures

Timed-pregnant BALB/c mice were obtained from Charles River (St. Constant, QC, Canada) and maintained according to institutional guidelines. Primary cortical cultures were prepared from 17-day-old fetuses as described previously.[36] In brief, the frontoparietal cortical area was dissected in Hanks' balanced salt solution supplemented with 15 mmol/L HEPES, 10 U/ml penicillin, and 10 μg/ml streptomycin and digested with 0.25% trypsin. A cell suspension was then prepared in Neurobasal medium supplemented with 1% fetal bovine serum, 2% B27, 50 μmol/L glutamine, 15 mmol/L HEPES, 10 U/ml penicillin, and 10 μg/ml streptomycin and neurons were plated at a density of 5 to 8 $\times$ 10^5 cells/ml in 6- or 96-well plates or on poly-D-lysine-coated coverslips. The medium was replaced 1 day later with the same medium without glutamine and fetal bovine serum. Five days after plating cortical neurons were treated with various concentrations (0.1 to 50 μg/ml) of U18666A for different periods of time (6 to 96 hours) and then processed to assess cholesterol accumulation, neuronal viability, and activity of cathepsins B and D. In a separate series of experiments, cultured cortical neurons were exposed to 5 μg/ml U18666A in the presence or absence of various concentrations of either cathepsin D inhibitor pepstatin A (1 to 50 μmol/L), cathepsin B inhibitor CA-074 methyl ester (0.05 to 1 μmol/L), or a combination of the two inhibitors. After a 24-hour incubation, cultured neurons were processed to detect the presence of glial cells and to measure neuronal viability, activity of cathepsins B and D, and subcellular distribution of these enzymes using the Qproteome Cell Compartment kit.

Viability of Cultured Neurons

Viability of neurons was assessed using a colorimetric assay that converts 3-(4,5-dimethylthiozolyl)-2,5-diphenyl-tetrazolium bromide (MTT) from yellow to a blue formazan crystal by dehydrogenase enzymes in metabolically active cells. In brief, control and treated neuronal culture medium from various experimental paradigms was replaced with new medium containing 0.25% MTT and cells were incubated for 2 hours in a CO_2 incubator at 37°C. The reaction was terminated, and cultures were assessed spectrophotometrically at 570 nm.[37] The experiment was repeated 3 times in triplicate. In a parallel series of experiments, neuronal apoptosis was assessed using the nuclear marker Hoechst 33258 as described earlier.[38] In brief, control and U18666A-treated cultures were fixed with 4% paraformaldehyde for 20 minutes, washed in PBS and then stained with Hoechst 33258 (50 ng/ml) for 10 minutes. The chromatin staining pattern was analyzed for individual cells under a Zeiss Axioskop-2 fluorescent microscope. The percentage of apoptotic cells was calculated by counting condensed/fragmented nuclei relative to the total number of cells. The data, which are presented as means $\pm$ SEM, were analyzed using one way analysis of variance followed by Dunnett's multiple comparisons test (GraphPad Software, San Diego, CA) with significance set at $P < 0.05$.

Determination of Lipid Mass

To determine cholesterol levels, hippocampal and cerebellar tissues from 4-, 7-, and 10-week-old *Npc1*$^{-/-}$ and control mice were homogenized and then digested for 2 hours at 30°C with phospholipase C. Tridecanoin (20 ng) was added as an internal standard, and lipids were extracted. The mass of cholesterol was determined using gas-liquid chromatography as described earlier.[39,40]

Filipin Staining

Filipin specifically labels unesterified cholesterol.[41] Sections from *Npc1*$^{-/-}$ and control mouse brains, as well as U18666A-treated cortical cultured neurons, were washed with 0.01 M PBS and then incubated in the dark with 125 μg/ml filipin in PBS for 3 hours under agitation at room temperature. Stained sections were examined using a Zeiss Axioskop-2 microscope.

Fluoro-Jade C Staining

Fluoro-Jade C labels degenerating neurons, dendrites, and axons.[42] Sections from *Npc1*$^{-/-}$ and control mouse brains were processed sequentially with 70% alcohol, distilled water, and 0.06% potassium permanganate solution. Subsequently, the sections were incubated with 0.0001% Fluoro-Jade C in 0.1% acetic acid for 10 minutes at room temperature, washed with distilled water, cleared with xylene, mounted, and examined using a Zeiss Axioskop-2 microscope.

Activity Assay of Cathepsins B and D

The hippocampus and cerebellum of 4-, 7-, and 10-week-old *Npc1*$^{-/-}$ and control mice (four to six animals per

group), as well as cultured mouse cortical neurons from various experimental paradigms, were homogenized on ice and then centrifuged (12,000 × *g*, 4°C, 10 minutes) to yield the supernatant. The protein was measured by a BCA protein assay kit (Pierce, Rockford, IL), equalized, and then activities of cathepsins B and D were measured using fluorogenic immunocapture activity assay kits according to the manufacturer's instructions.

Electron Microscopy

Parasagittal sections from the cerebellum and coronal sections from the hippocampus were cut on a Vibratome (200 μm), postfixed in 2% osmium tetroxide and 3% FeCN for 1 hour at 4°C, washed in maleate buffer (pH 6), counterstained in 1% uranyl acetate, washed in maleate buffer, dehydrated in ascending alcohol, and embedded in Araldite. Ultrathin sections (80 nm) were cut on an ultramicrotome (Leica EMUC6) and then collected on uncoated nickel grids. Sections were further counterstained with uranyl acetate and lead citrate before observation with a transmission electron microscope (CM10, Philips, Eindhoven, The Netherlands) as described earlier.[43] Ten Purkinje cells and 10 pyramidal neurons from both *Npc1*$^{-/-}$ and *Npc1*$^{+/+}$ mice were randomly chosen under the electron microscope and subjected to quantification. The number of lysosomes/cytoplasmic area for each cell was calculated using ImageJ software (NIH, Bethesda, MD). Differences between *Npc1*$^{-/-}$ and *Npc1*$^{+/+}$ Purkinje cells and pyramidal cells were examined for statistical significance using one-way analysis of variance with an unpaired Student's *t* test with significance set at $P < 0.001$. The data are expressed as mean ± SEM for each group.

Immunoblotting

Brain tissues (cortex, hippocampus, and cerebellum) from *Npc1*$^{-/-}$ and control mice of 4, 7, and 10 weeks of age (four to six animals per group) were homogenized in ice-cold radioimmunoprecipitation assay-lysis buffer (20 mmol/L Tris-HCl [pH 8], 150 mmol/L NaCl, 0.1% SDS, 1 mmol/L EDTA, 1% Igepal CA-630, 50 mmol/L NaF, 1 mmol/L $NaVO_3$, 10 μg/ml leupeptin, and 10 μg/ml aprotinin). The proteins were separated by 4 to 20% polyacrylamide gel electrophoresis and then transferred to nitrocellulose membranes. The membranes were blocked for 1 hour with 5% nonfat milk in 10 mmol/L Tris-HCl (pH 8.0), 150 mmol/L NaCl, and 0.2% Tween 20 (TBST), and incubated overnight at 4°C with anti-cathepsin D (1:200), anti-cathepsin B (1:200), anti-IGF-II/M6P receptor (1:1000), anti-LC3 (1:500), and anti-beclin-1 (1:200) antibodies. Membranes were then incubated with appropriate horseradish peroxidase-conjugated secondary antibodies (1:5000), and immunoreactive proteins were visualized using an ECL detection kit. Blots were subsequently reprobed with anti-β-actin (1:1000) and quantified using an MCID image analysis system.[44] The levels of various markers were normalized to β-actin present in each band. The data, which are presented as means ± SEM, were analyzed using one-way analysis of variance followed by Newman-Keuls post hoc analysis with significance set at $P < 0.05$.

Immunostaining

Brain sections from different age groups of *Npc1*$^{-/-}$ and control mice (three to five animals per group) were processed following the free-floating procedure as described earlier.[45,46] For the enzyme-linked procedure, 40-μm sections were washed in PBS, treated with 1% hydrogen peroxide for 30 minutes, and then incubated overnight at room temperature with rabbit anti-IGF-II/M6P receptor (1:3000), goat anti-cathepsin D (1:200), or goat-anti-cathepsin B (1:200) antiserum. Sections were then washed with PBS, exposed to horseradish peroxidase-conjugated secondary antibodies for 1 hour, and developed using the glucose oxidase-nickel enhancement method. Immunostained sections were examined and photographed using a Zeiss Axioskop-2 microscope.

For double immunofluorescence staining, 20 μm brain sections from *Npc1*$^{-/-}$ and control mice of different age groups were incubated overnight with a combination of anti-IGF-II/M6P receptor (1:1000), anti-cathepsin D (1:200), anti-cathepsin B (1:200), anti-Iba1 (1:1500), anti-GFAP (1:1000) or anti-cleaved caspase-3 (1:200), anti-myelin associated glycoprotein (1:200), FITC-tagged lectin (1:500), anti-calbindin (1:3000) antisera, or NeuroTrace (1:300). Because anti-IGF-II/M6P receptor and anti-Iba1 antisera were raised in rabbit, we used FITC-tagged lectin along with anti-IGF-II/M6P receptor antiserum to establish the possible localization of the receptor on the activated microglia. After incubation, sections were rinsed with PBS, exposed to Texas Red- or FITC-conjugated secondary antibodies (1:200) for 2 hours at room temperature, washed, and coverslipped with Vectashield mounting medium. In a parallel series of experiment, cortical cultured neurons were first labeled with anti-GFAP (1:1000) or anti-Iba1 (1:500) and then stained with the neuronal marker NeuroTrace (1:300). Immunostained sections were examined under a Zeiss Axioskop-2 fluorescence microscope, and photomicrographs were taken with a Nikon 200 digital camera.

Subcellular Fractionation

The hippocampus, cortex, and cerebellum of 4-, 7-, and 10-week-old *Npc1*$^{-/-}$ and control mice (four to six animals per group) were homogenized in cold PBS and then fractionated, using the Qproteome Cell Compartment kit, into cytoskeletal, cytosol, membrane, and nuclear proteins. Subcellular fractions were equalized and immunoblotted with anti-cathepsin D (1:200), anti-cathepsin B (1:200), anti-Bax2 (1:200), anti-AIF (1:200), or anti-cytochrome *c* (1:1000) antiserum. In a separate series of experiments, cultured mouse cortical neurons from various experimental paradigms were homogenized, fractionated using the Qproteome Cell Compartment kit and then processed for immunoblotting with anti-cathepsin D (1:200) and anti-cathepsin B (1:200) antibodies. Membranes from both experiments were then washed with

TBST, incubated with appropriate horseradish peroxidase-conjugated secondary antibodies (1:5000), and visualized using an ECL detection kit. Blots were subsequently reprobed with anti-N cadherin (1:200), anti-glyceraldehyde-3-phosphate dehydrogenase (1:1000), anti-histone (1:1000), or anti-β-actin (1:1000) antisera. In a parallel series of experiment, the hippocampus and cerebellum of 7-week-old *Npc1*$^{-/-}$ and control mice (two animals per group) were homogenized in cold PBS and fractionated using the lysosomal isolation kit into lysosomal and cytosolic fractions. The proteins were equalized, processed for Western blotting using either anti-cathepsin B (1:200) or anti-cathepsin D (1:200) antibodies and then reprobed with anti-lysosomal associated membrane protein 2 antiserum as described above. All blots were quantified using an MCID image analysis system[33] and the data, which are presented as means ± SEM, were analyzed using one-way analysis of variance followed by Newman-Keuls post hoc analysis with significance set at $P < 0.05$.

Results

Altered Cholesterol Distribution and Loss of Neurons in *Npc1*$^{-/-}$ Mice

In keeping with earlier results,[41,47] filipin-labeled cholesterol was evident in almost all neurons of the hippocampus, cortex, and cerebellum of *Npc1*$^{-/-}$ mice. The total cholesterol content, on the other hand, was not significantly different either in the hippocampus or cerebellum of *Npc1*$^{-/-}$ mice compared with controls in any age group (Supplemental Figures S1 and S2, see *http://ajp.amjpathol.org*). It is possible that cholesterol mass, as reported by Karten et al,[47] may accumulate in cell bodies and is reduced in axons of NPC1-deficient neurons. We then assessed the degeneration of neurons by Fluoro-Jade C and cleaved caspase-3 staining and evaluated the levels of two well established autophagy markers, LC3 and beclin-1, in the hippocampal and cerebellar regions of 4-, 7-, and 10-week-old *Npc1*$^{-/-}$ and control mice. Our results showed Fluoro-Jade C and cleaved caspase-3-labeled cells in the cerebellum but not in the hippocampus of the *Npc1*$^{-/-}$ mouse brains. Some Fluoro-Jade C-labeled neurons were also apparent in the prefrontal cortical region of the *Npc1*$^{-/-}$ mouse brains (Supplemental Figures S1 and S2, see *http://ajp.amjpathol.org*). More of these degenerating cells were present at 4 and 7 weeks, but very few were observed in the 10-week-old cerebellum of *Npc1*$^{-/-}$ mouse brains. As for the autophagy marker LC3, it is known that after induction of autophagy this protein is modified from its cytosolic LC3-I form to a rapidly migrating, lipid-conjugated LC3-II form associated with autophagosomal membranes.[48,49] Beclin-1, on the other hand, is part of the class III phosphatidyl-inositol-3 kinase complex that participates in autophagosome formation.[50] Our results showed that levels of LC3-II and, to some extent, those of beclin-1 are increased in both the cerebellum and hippocampus of *Npc1*$^{-/-}$ mice compared with controls (Supplemental Figure S1, see *http://ajp. amjpathol.org*). Concomitant with the loss of neurons, we observed an up-regulation of reactive astrocytes and activated microglia in the hippocampus and cerebellum of *Npc1*$^{-/-}$ mice compared with age-matched controls. In addition, the density of myelinated fibers progressively decreased between 4 and 10 weeks in the *Npc1*$^{-/-}$ mouse brains (Supplemental Figure S1, see *http://ajp.amjpathol.org*).

Altered Lysosomes in *Npc1*$^{-/-}$ Mice

To determine whether lysosomes, the major site of cholesterol accumulation in NPC1-deficient cells, are differentially altered in NPC pathology, we evaluated ultrastructural features of hippocampal neurons and cerebellar Purkinje cells in *Npc1*$^{-/-}$ and *Npc1*$^{+/+}$ mice using conventional electron microscopic procedures (Figure 1, A–E). Both hippocampal and cerebellar neurons in *Npc1*$^{+/+}$ mice display no obvious morphological changes (Figure 1, A and C). These neurons contained rare primary lysosomes (see insets) characterized by a homogeneous electron-dense granular content. In *Npc1*$^{-/-}$ mice the Purkinje cells were shrunken and clearly distinguishable on the basis of their intense electron density. The cell body contained severe cytoplasmic vacuolization and a dark nucleus (Figure 1D). The pyramidal neurons, on the other hand, were less severely affected, with mild cytoplasm vacuolization and no signs of nuclear alterations (Figure 1B). Interestingly, the number and area occupied by secondary lysosomes with heterogeneous dark content and numerous concentric lamellar bodies were increased in both hippocampal and cerebellar neurons in *Npc1*$^{-/-}$ mice, but it was more striking in Purkinje cells than in pyramidal neurons (Figure 1, B, D, and E).

Lysosomal Enzymes in *Npc1*$^{-/-}$ Mice

To examine the possible involvement of lysosomal enzymes in NPC pathology, we evaluated the levels, activity, and expression of cathepsin B (Figures 2 and 3, Supplemental Figure S2, see *http://ajp.amjpathol.org*) and cathepsin D (Figures 4 and 5, Supplemental Figure S2, see *http://ajp.amjpathol.org*) in the hippocampus, cerebellum, and cortex of 4-, 7-, and 10-week-old *Npc1*$^{-/-}$ mice compared with controls. Our data revealed that cathepsin B (Figures 2, A–C, and 3, A–C, Supplemental Figure S2, see *http://ajp.amjpathol.org*) and cathepsin D (Figures 4, A–C, and 5, A–C, Supplemental Figure S2, see *http://ajp.amjpathol.org*) levels and activity were significantly higher in the hippocampus, cerebellum, and cortex of *Npc1*$^{-/-}$ mice compared with those in age-matched controls. Notably, the changes were more prominent in the cerebellum and cortex than in the hippocampus of the *Npc1*$^{-/-}$ mice at all ages.

At the cellular level, cathepsin B and D immunoreactivity in control mice was widely but selectively distributed, mostly in neurons of the brain. The hippocampal formation exhibited intense lysosomal enzyme immunoreactivity, primarily in CA1 to CA3 pyramidal neurons and

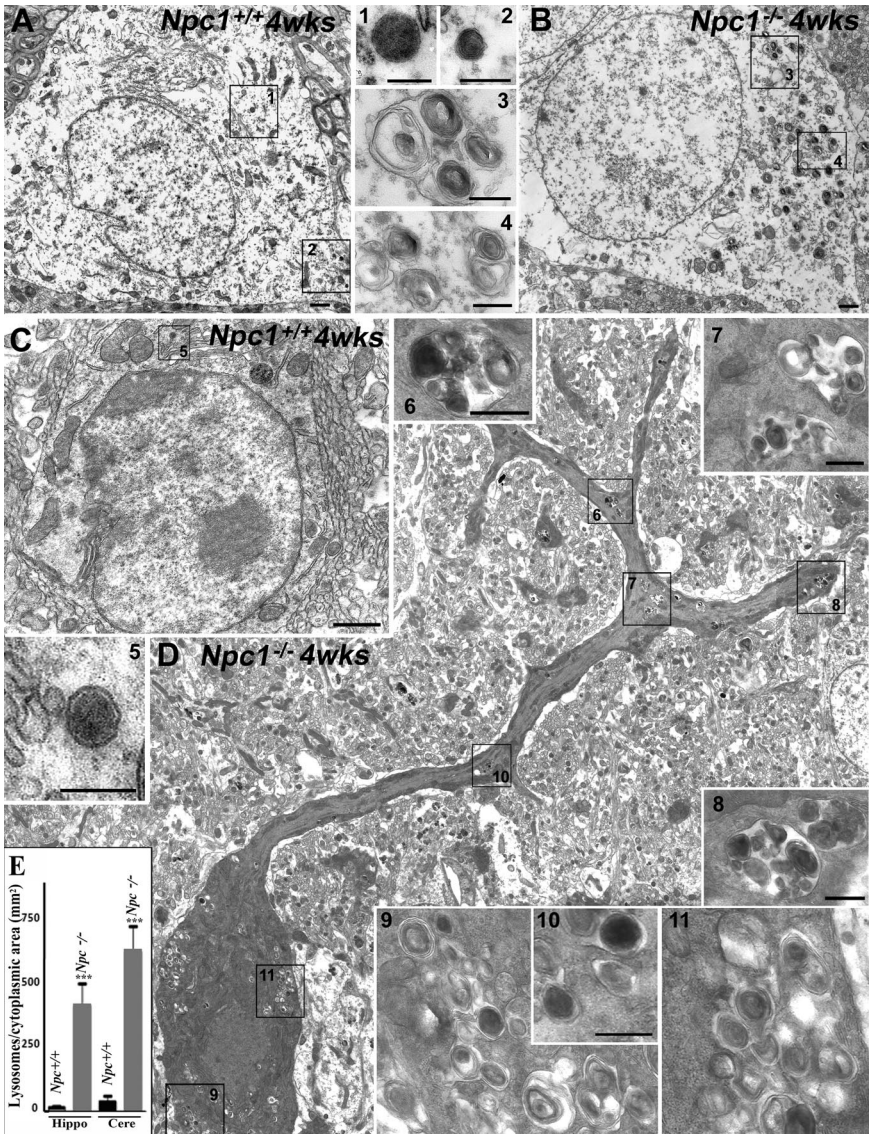

Figure 1. A and **B:** Photomicrographs showing the ultrastructure of hippocampal pyramidal cells in 4-week-old (wks) control (*Npc1*$^{+/+}$; **A**) and *Npc1*$^{-/-}$ (**B**) mice. In *Npc1*$^{+/+}$ mice (**A**) the pyramidal cell shows the classical ultrastructural morphology characterized by large round nucleus surrounded by a clear cytoplasm containing organelles and sparse primary lysosomes (**insets 1** and **2**). In *Npc1*$^{-/-}$ mice (**B**) there is no evidence of cell degeneration, but the number of lysosomes is relatively higher, and they are characterized by dense concentric lamellar bodies of various sizes and densities (**insets 3** and **4**). The areas indicated by the rectangles and the numbers are shown at higher magnification in the **insets**. **C** and **D:** Photomicrographs showing the ultrastructure of cerebellar Purkinje cells in 4-week-old control (*Npc1*$^{+/+}$; **C**) and *Npc1*$^{-/-}$ (**D**) mice. In *Npc1*$^{+/+}$ mice (**C**) a Purkinje cell shows the classic ultrastructural morphology characterized by a round large nucleus, a clear cytoplasm with organelles, and sparse primary lysosomes (**inset 5**). In *Npc1*$^{-/-}$ mice (**D**) note the evident degeneration of the cell characterized by nuclear condensation and accumulation of lysosomes and vacuoles. Both primary (**inset 10**) and secondary lysosomes are present in the cytoplasm. In particular, note the large secondary lysosomes with heterogeneous dark content, dense concentric lamellar bodies, and granules of various sizes and densities (**insets 6–8** and **9–11**). The areas indicated by the rectangles and the numbers are shown at higher magnification in the **insets**. **E:** Histograms showing the number of lysosomes/cytoplasmic area in hippocampus and cerebellum of *Npc1*$^{+/+}$ and *Npc1*$^{-/-}$ mice. A significant increase in the number of lysosomes was observed in the hippocampus and cerebellum of *Npc1*$^{-/-}$ mice. The increase is more evident in Purkinje cells than in pyramidal cells. Hippo, hippocampus; Cere, cerebellum. Scale bars: 1 μm (**A** and **B**); 250 nm (**insets 1–4**); 1 μm (**C** and **D**); 250 nm (**inset 5**); 500 nm (**insets 6–8/9** and **11**); 250 nm (**inset 10**). ***$P < 0.001$.

granule cells of the dentate gyrus. Occasionally, cathepsin B- and D-immunoreactive neurons were apparent in the strata oriens and stratum radiatum along with strongly labeled polymorphic neurons in the hilus region of the dentate gyrus (Figures 2D and 4D). Lysosomal enzyme immunoreactivity was detected in all layers of the cortex with varying degrees of intensity, including high expression in layers IV to VI and moderate expression in layers II to III (Supplemental Figure S2, see *http://ajp.amjpathol.org*). In the cerebellar region, most Purkinje cells and neurons of the deep cerebellar nuclei showed high levels of cathepsins B and D expression, whereas the granule cell layer displayed moderate immunoreactivity in control brains (Figures 3D and 5D). In *Npc1*$^{-/-}$ mouse brains, cathepsin B (Figures 2, E and F, and 3, E and F, Supplemental Figure S2, see *http://ajp.amjpathol.org*) and cathepsin D (Figures 4, E and F, and 5, E and F, Supplemental Figure S2, see *http://ajp.amjpathol.org*) immunoreactivity was evident in hippocampal, cortical, and cerebellar neurons as well as in glial cells. In some neurons lysosomal enzyme immunoreactivity was confined to the apical regions of the cell soma. In addition, a moderate increase in cathepsin B and D immunoreactivity was noted in the neurons of the hippocampus, cortex, and deep cerebellar nuclei as well as in Purkinje cells in *Npc1*$^{-/-}$ mice compared with controls. At the cellular level, cathepsin B and D immunoreactivity in cerebellar Purkinje cells seemed to be more punctate in control compared with *Npc1*$^{-/-}$ mouse brains (Supplemental Figure S3, see *http://ajp.amjpathol.org*). The cerebellar granule cells, on the other hand, did not exhibit any marked alteration in lysosomal enzyme immunoreactivity. Our double-labeling studies further revealed that all activated microglia, but not reactive astrocytes, in the hippocampal, cortical, and cerebellar regions of *Npc1*$^{-/-}$ mouse brains expressed cathepsin B (Figures 2, G–R, and 3, G–R, Supplemental Figure S2, see *http://ajp.amjpathol.org*) and cathepsin D (Figures 4, G–R, and 5, G–R, Supplemental Figure S2, see *http://ajp.amjpathol.org*).

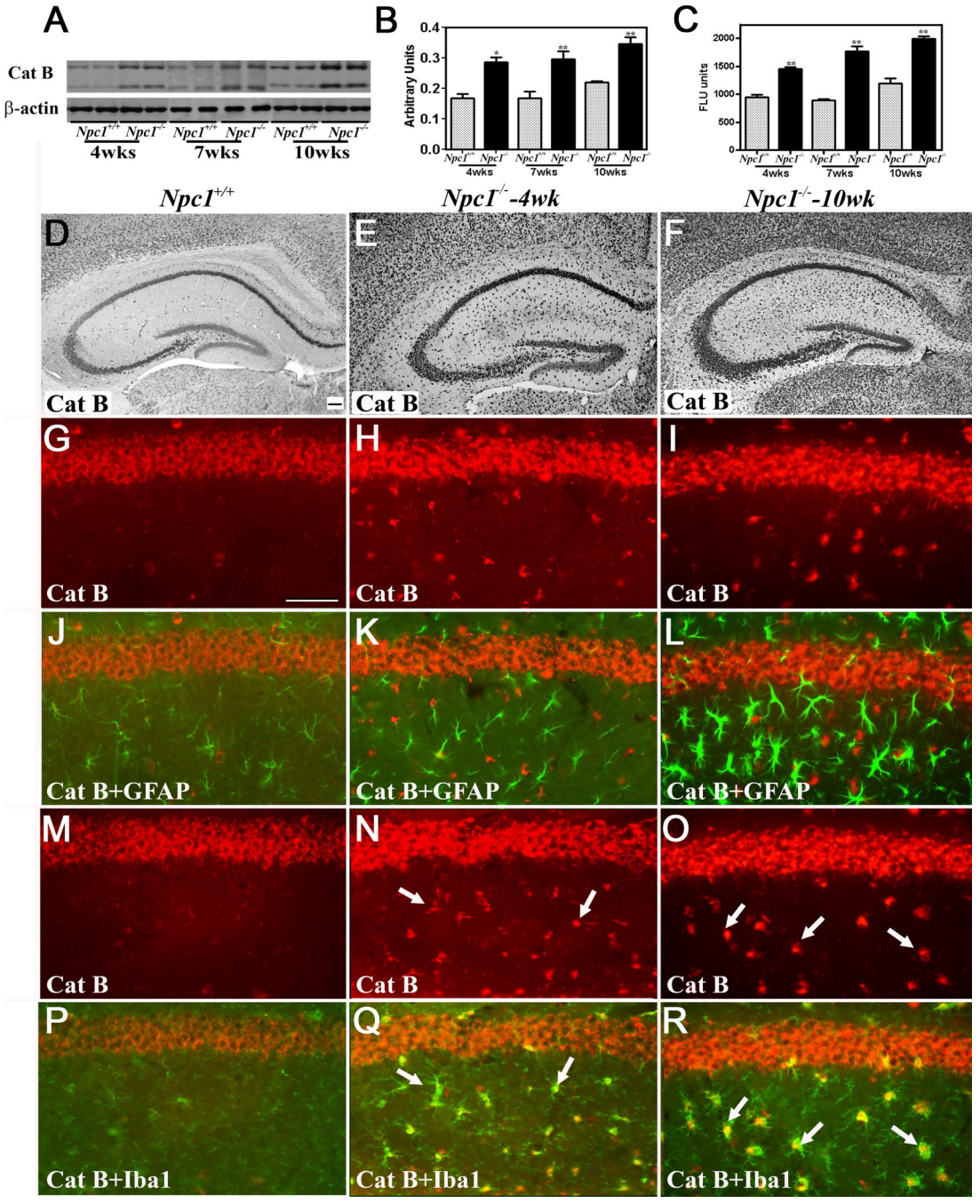

Figure 2. A–C: Immunoblot (**A** and **B**) and enzyme activity (**C**) assays showing increased levels and activity of cathepsin B in the hippocampus of 4-, 7- and 10-week-old (wks) *Npc1*$^{-/-}$ mouse brains compared with age-matched controls (*Npc1*$^{+/+}$). Histograms represent quantification of cathepsin B levels/activity from at least three separate experiments, each of which was replicated two to three times. **D–F:** Photomicrographs showing the cellular distribution of the cathepsin B in the hippocampus of the control (*Npc1*$^{+/+}$; **D**) and 4-week-old (**E**) and 10-week-old (**F**) *Npc1*$^{-/-}$ mice. Note the relative change in intensity and distribution of cathepsin B immunoreactivity in the hippocampus of *Npc1*$^{-/-}$ mouse brains. **G–R:** Double immunofluorescence photomicrographs of control (*Npc1*$^{+/+}$; **G, J, M,** and **P**) and 4-week-old (**H, K, N,** and **Q**) and 10-week-old (**I, L, O,** and **R**) *Npc1*$^{-/-}$ mouse hippocampus showing the possible colocalization of cathepsin B (**G–I** and **M–O**) with GFAP-labeled astrocytes (**J–L**) and Iba1-labeled microglia (**P–R**). In *Npc1*$^{-/-}$ hippocampus a number of microglia (**N, Q, O,** and **R**) but not astrocytes (**H, K, I,** and **L**) exhibit cathepsin B immunoreactivity (**arrows**). Cat B, cathepsin B. Scale bar = 25 μm. $^{*}P < 0.05$; $^{**}P < 0.01$.

IGF-II/M6P Receptor in Npc1$^{-/-}$ *Mice*

Earlier studies have shown that after their synthesis in the endoplasmic reticulum, lysosomal enzymes are transported to the EL system by binding to the IGF-II/M6P receptor.[22–24] To determine whether altered lysosomal enzyme levels in *Npc1*$^{-/-}$ mice are associated with parallel changes in IGF-II/M6P receptors, we examined the level/expression of the receptor in the hippocampus and cerebellum of *Npc1*$^{-/-}$ mice (Figure 6). Western blotting showed that the IGF-II/M6P receptor did not exhibit any significant alterations either in the hippocampus or cerebellum of *Npc1*$^{-/-}$ mice at any stage (Figure 6, A–D).

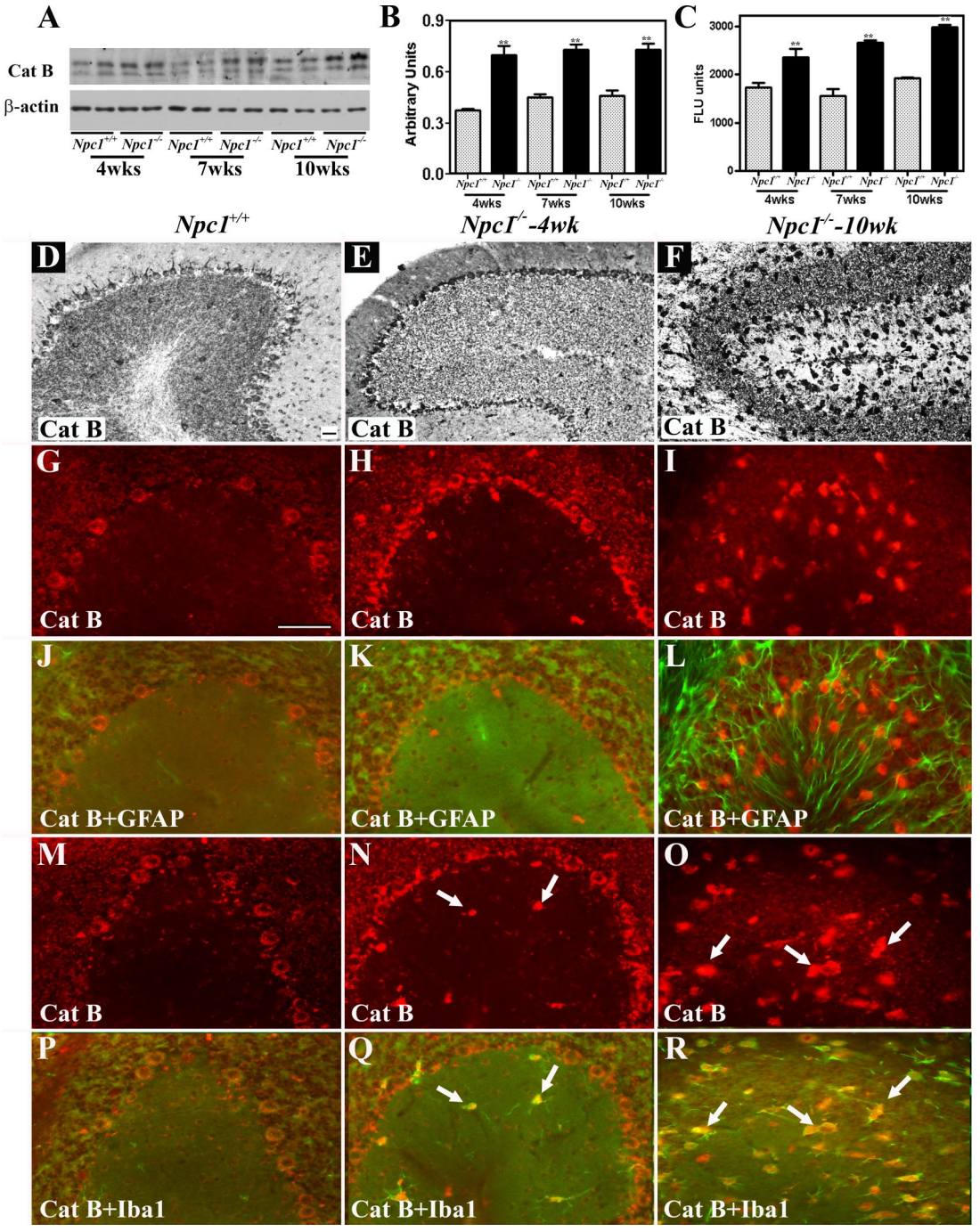

Figure 3. A–C: Immunoblot (**A** and **B**) and enzyme activity (**C**) assays showing increased levels and activity of cathepsin B in the cerebellum of 4-, 7-, and 10-week-old (wks) *Npc1*$^{-/-}$ mouse brains compared with age-matched controls (*Npc1*$^{+/+}$). Histograms represent quantification of cathepsin B levels/activity from at least three separate experiments, each of which was replicated two to three times. **D–F:** Photomicrographs showing the cellular distribution of the cathepsin B in the cerebellum of the control (*Npc1*$^{+/+}$; **D**) and 4-week-old (**E**) and 10-week-old (**F**) *Npc1*$^{-/-}$ mice. Note the relative change in intensity and distribution of cathepsin B immunoreactivity in the cerebellum of *Npc1*$^{-/-}$ mouse brains. **G–R:** Double immunofluorescence photomicrographs of control (*Npc1*$^{+/+}$; **G, J, M,** and **P**) and 4-week-old (**H, K, N,** and **Q**) and 10-week-old (**I, L, O,** and **R**) *Npc1*$^{-/-}$ mouse cerebellum showing the possible colocalization of cathepsin B (**G–I** and **M–O**) with GFAP-labeled astrocytes (**J–L**) and Iba1-labeled microglia (**P–R**). In *Npc1*$^{-/-}$ cerebellum a number of microglia (**N, Q, O,** and **R**) but not astrocytes (**H, K, I,** and **L**) exhibit cathepsin B immunoreactivity (**arrows**). Cat B, cathepsin B. Scale bar = 25 μm. $^{**}P < 0.01$.

At the cellular level, IGF-II/M6P receptor immunoreactivity in control mouse brains was evident primarily in the neurons. In the hippocampus, intense receptor immunoreactivity was apparent in the CA1 to CA3 pyramidal cell layer (Figure 6E) and in a few medium-sized neurons scattered in the strata oriens and stratum radiatum. Within the dentate gyrus, granule cell somata were outlined by a fine mesh of weakly stained puncta and occasional strongly labeled neurons (Figure 6E). In the cerebellum, immunoreactivity was evi-

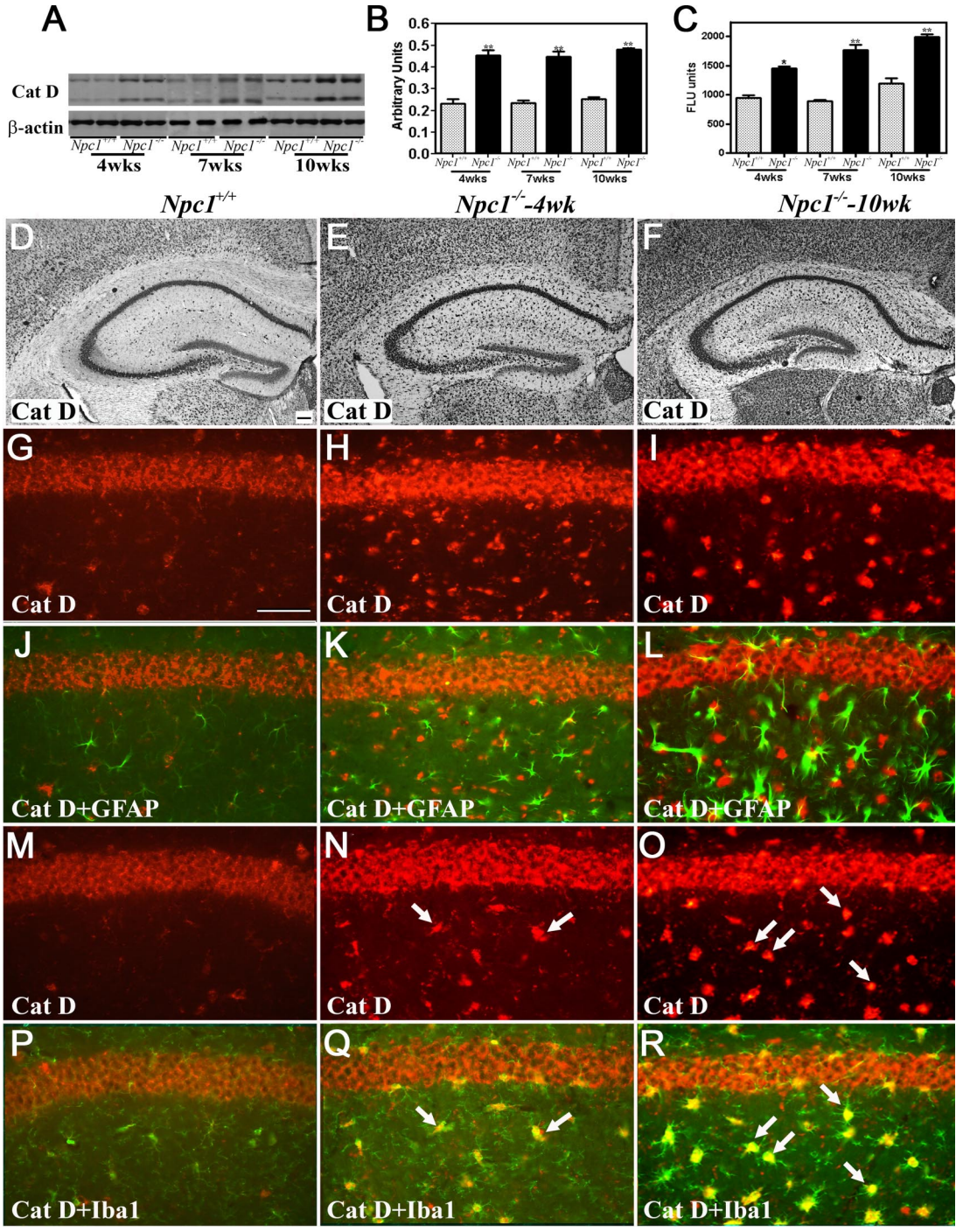

Figure 4. A–C: Immunoblots (**A** and **B**) and enzyme activity (**C**) assays showing increased levels and activity of cathepsin D in the hippocampus of 4-, 7-, and 10-week-old (wks) $Npc1^{-/-}$ mouse brains compared with age-matched controls ($Npc1^{+/+}$). Histograms represent quantification of cathepsin D levels/activity from at least three separate experiments, each of which was replicated two to three times. **D–F:** Photomicrographs showing the cellular distribution of the cathepsin D in the hippocampus of the control ($Npc1^{+/+}$; **D**) and 4-week-old (**E**) and 10-week-old (**F**) $Npc1^{-/-}$ mice. Note the relative change in intensity and distribution of cathepsin D immunoreactivity in the hippocampus of $Npc1^{-/-}$ mouse brains. **G-R:** Double immunofluorescence photomicrographs of control ($Npc1^{+/+}$; **G, J, M,** and **P**) and 4-week-old (**H, K, N,** and **Q**) and 10-week-old (**I, L, O,** and **R**) $Npc1^{-/-}$ mouse hippocampus showing the possible colocalization of cathepsin D (**G–I** and **M–O**) with GFAP-labeled astrocytes (**J–L**) and Iba1-labeled microglia (**P–R**). In $Npc1^{-/-}$ hippocampus a number of microglia (**N, Q, O,** and **R**) but not astrocytes (**H, K, I,** and **L**) exhibit cathepsin D immunoreactivity (**arrows**). Cat D, cathepsin D. Scale bar = 25 μm. $^{*}P < 0.05$; $^{**}P < 0.01$.

dent in the Purkinje cells as well as the granule cell layer (Figure 6F). Double immunolabeling experiments of control mouse brains revealed that i) IGF-II/M6P receptor colocalized with all cathepsin-positive neurons in both the hippocampus (Figure 6, I and J) and cerebellum (Figure 6, K and L), and ii) occasionally some astrocytes, but not microglia, expressed the receptor (data not shown). In contrast with controls, we observed a decrease in IGF-II/M6P receptor immunoreactivity in neurons of 7- and 10-week-old $Npc1^{-/-}$

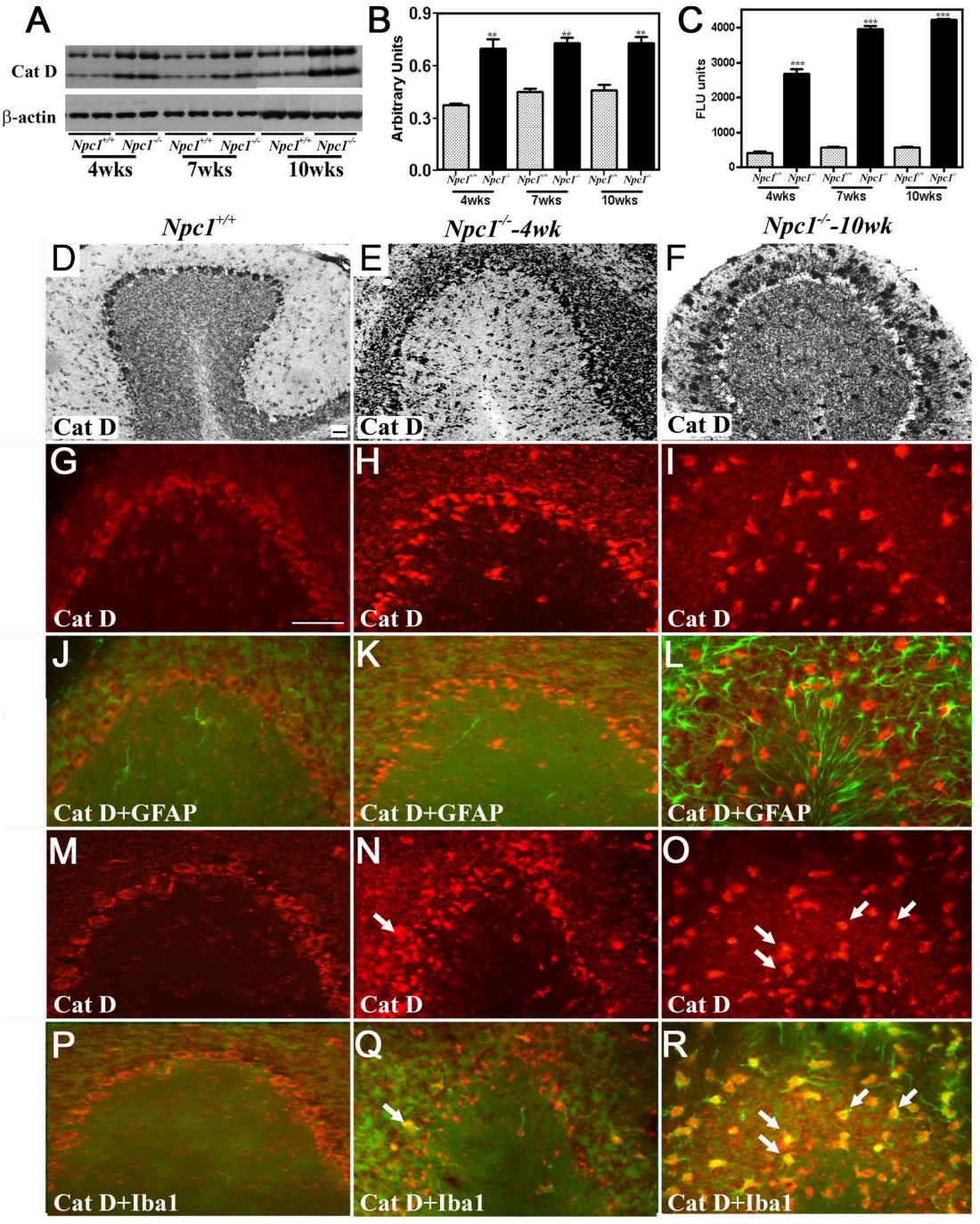

Figure 5. A–C: Immunoblots (**A** and **B**) and enzyme activity (**C**) assays showing increased levels and activity of cathepsin D in the cerebellum of 4-, 7-, and 10-week-old (wks) old *Npc1*$^{-/-}$ mouse brains compared with age-matched controls (*Npc1*$^{+/+}$). Histograms represent quantification of cathepsin D levels/activity from at least three separate experiments, each of which was replicated two to three times. **D–F:** Photomicrographs showing the cellular distribution of the cathepsin D in the cerebellum of the control (*Npc1*$^{+/+}$; **D**) and 4-week-old (**E**) and 10-week-old (**F**) *Npc1*$^{-/-}$ mice. Note the relative change in intensity and distribution of cathepsin D immunoreactivity in the cerebellum of *Npc1*$^{-/-}$ mouse brains. **G-R:** Double immunofluorescence photomicrographs of control (*Npc1*$^{+/+}$; **G, J, M,** and **P**) and 4-week-old (**H, K, N,** and **Q**) and 10-week-old (**I, L, O,** and **R**) *Npc1*$^{-/-}$ mouse cerebellum showing the possible colocalization of cathepsin D (**G–I** and **M–O**) with GFAP-labeled astrocytes (**J–L**) and Iba1-labeled microglia (**P–R**). In *Npc1*$^{-/-}$ cerebellum a number of microglia (**N, Q, O,** and **R**) but not astrocytes (**H, K, I,** and **L**) exhibit cathepsin D immunoreactivity (**arrows**). Cat D, cathepsin D. Scale bar = 25 μm. $^{**}P < 0.01$; $^{***}P < 0.001$.

mice (Figure 6, G and H). In addition, the majority of reactive astrocytes (Figure 6, O, P, S, and T) but not activated microglia (Figure 6, M, N, Q, and R), located in the hippocampus and cerebellum of *Npc1*$^{-/-}$ mice, showed IGF-II/M6P receptor immunoreactivity.

Lysosomal Enzymes and Loss of Neurons in Npc1$^{-/-}$ *mice*

A number of studies have shown that up-regulation of lysosomal enzymes may represent a protective response

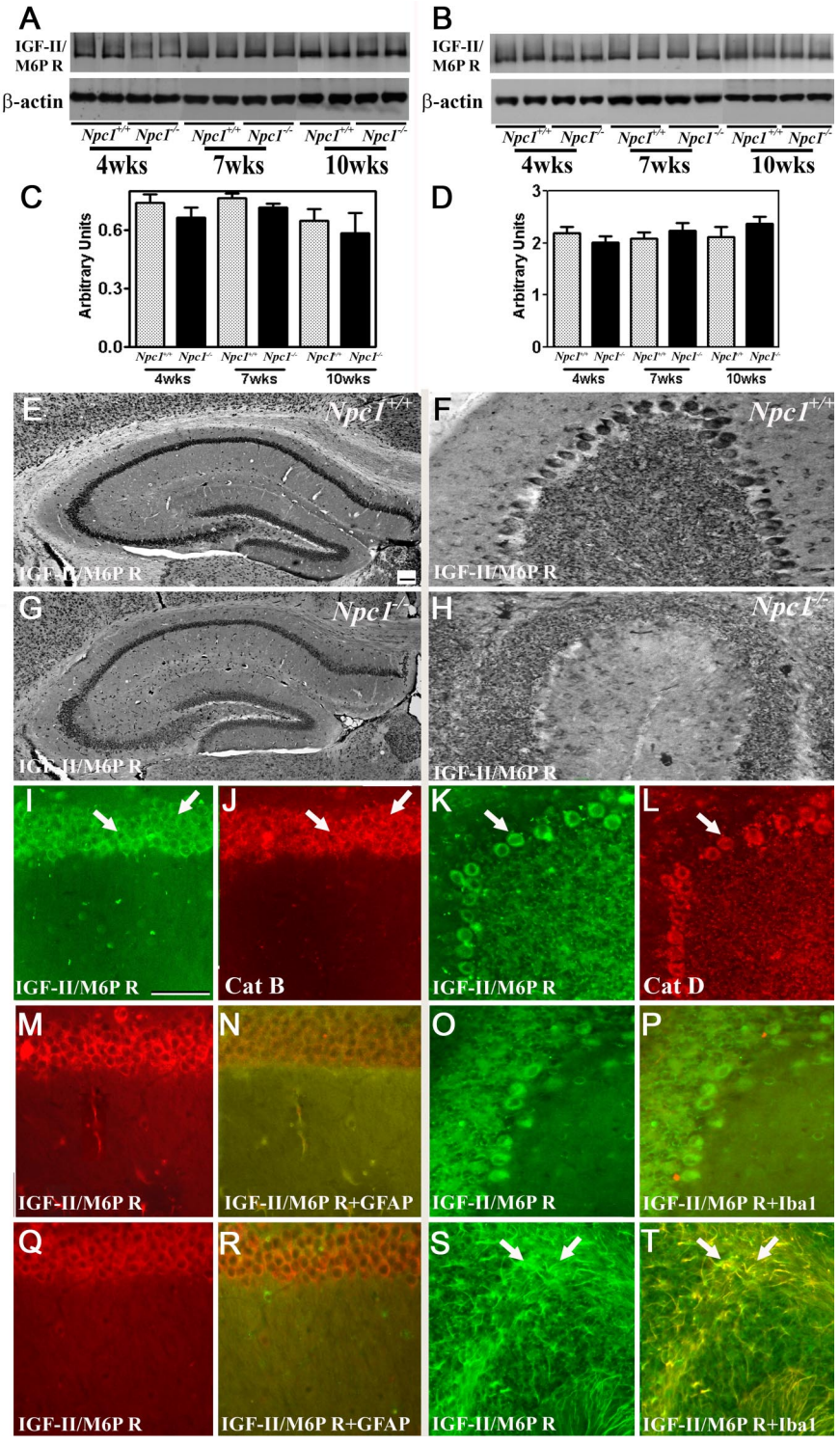

Figure 6. A–D: Immunoblots and respective histograms showing that IGF-II/M6P receptor levels are not significantly altered in the hippocampus (**A** and **C**) or cerebellum (**B** and **D**) of 4-, 7-, and 10-week-old (wks) *Npc1*$^{-/-}$ mouse brains compared with age-matched controls (*Npc1*$^{+/+}$). Histograms represent quantification of the IGF-II/M6P receptor level from at least three separate experiments, each of which was replicated two to three times. **E–H:** Photomicrographs showing the cellular distribution of the IGF-II/M6P receptor in the hippocampus (**E** and **G**) and cerebellum (**F** and **H**) of the control (*Npc1*$^{+/+}$; **E** and **F**) and 10-week-old (**G** and **H**) *Npc1*$^{-/-}$ mice. Note the relative change in intensity and distribution of the IGF-II/M6P receptor immunoreactivity in the hippocampus and cerebellum of *Npc1*$^{-/-}$ mouse brains. **I–L:** Double immunofluorescence photomicrographs of control mouse hippocampus (**I** and **J**) and cerebellum (**K** and **L**) showing the colocalization (**arrows**) of the IGF-II/M6P receptor (**I** and **K**) with cathepsin B (**J**) and cathepsin D (**L**) immunoreactivity. **M–T:** Double immunofluorescence photomicrographs of control (*Npc1*$^{+/+}$; **M, N, O,** and **P**) and 10-week-old (**Q, R, S,** and **T**) *Npc1*$^{-/-}$ mouse hippocampus (**M, N, Q,** and **R**) and cerebellum (**O, P, S,** and **T**) showing the possible colocalization of the IGF-II/M6P receptor (**M, Q, O,** and **S**) with lectin-labeled microglia (**N** and **R**) and GFAP-labeled astrocytes (**P** and **T**). A number of astrocytes (**S** and **T**)(**arrows**) but not microglia (**Q** and **R**) exhibit IGF-II/M6P receptor immunoreactivity in *Npc1*$^{-/-}$ mice. Cat B, cathepsin B; Cat D, cathepsin D. IGF-II/M6PR, IGF-II/M6P receptor. Scale bar = 25 μm.

to overcome abnormal protein accumulation, or alternatively may lead to loss of cell viability. In general, increased enzyme activity within lysosomes or limited release of enzymes into the cytosol can prevent sublethal damage,[32,33,51] whereas lysosomal rupture or membrane destabilization, leading to sustained release of enzymes into the cytosol, can induce cell death directly or indirectly via cytochrome c release from mitochondria.[20,28,52] Once in the cytosol, cytochrome *c* associates with Apaf-1, forming an apoptosome complex that, in the presence of dATP/ATP, is capable of activating caspase-9 followed by caspase-3, leading to cell death.[51,53,54] Lysosomal enzymes can induce mitochondrial permeability either by activating phospholipase A2[55] or by cleaving the Bcl-2 family member Bid, which in its truncated form translocates to mitochondria, resulting in Bax/Bak activation.[56,57] There is also evidence that dam-

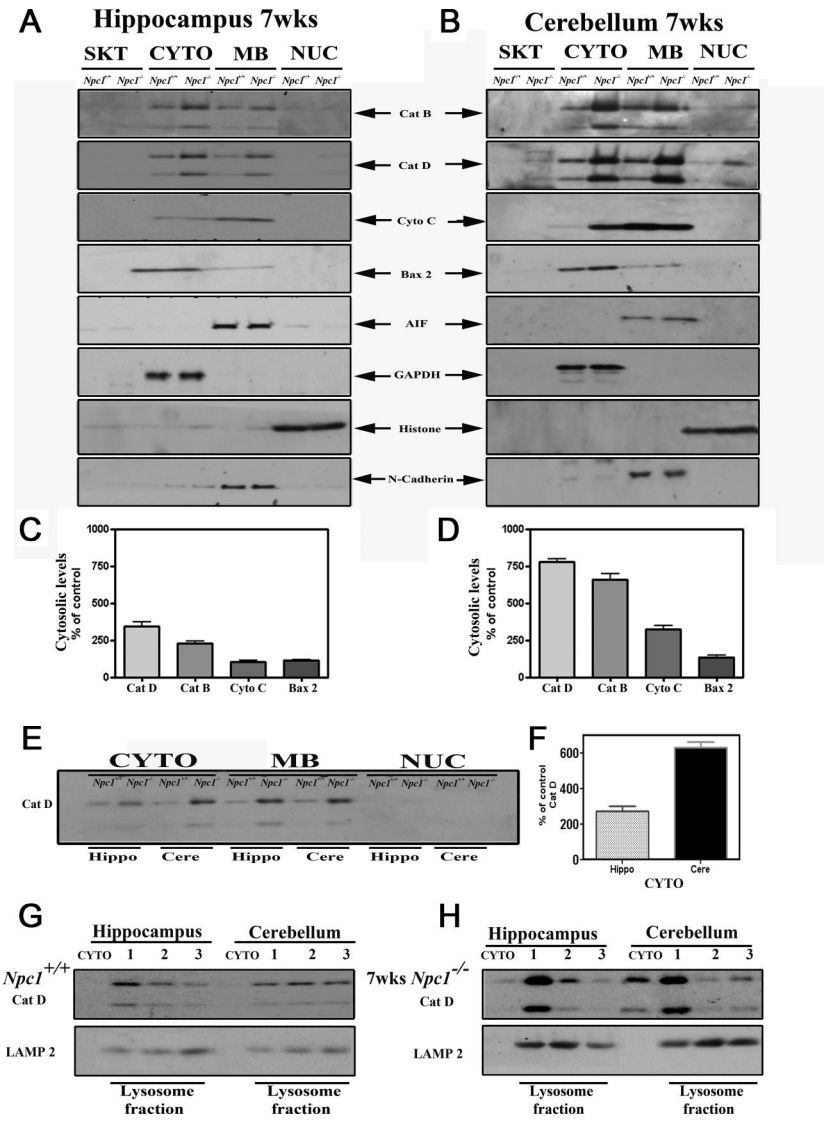

Figure 7. A–D: Immunoblots (**A** and **B**) and respective histograms (**C** and **D**) showing subcellular distribution of cathepsin B, cathepsin D, cytochrome *c*, Bax2, and AIF in the hippocampus and cerebellum of 7-week-old control and *Npc1*$^{-/-}$ mice. The subcellular fractions were prepared using Qproteome Cell Compartment kit. Note the relatively higher cytosolic levels of cathepsins, cytochrome *c*, and Bax2 in the cerebellum compared with hippocampus. No marked alterations in AIF levels were evident in *Npc1*$^{-/-}$ mice compared with controls. Histograms represent quantification of cathepsins, cytochrome *c*, and Bax2 levels from at least three separate experiments, each of which was replicated two times. **E** and **F:** Immunoblot and corresponding histogram showing changes in the subcellular levels of cathepsin D in the hippocampus and cerebellum of 7-week-old control and *Npc1*$^{-/-}$ mouse brains run on the same gel. Note the relative increase in the cytosolic cathepsin D level in the cerebellum compared with that in the hippocampus. **G** and **H:** Immunoblot showing cytosolic and lysosomal levels of cathepsin D in the hippocampus and cerebellum of 7-week-old control (**G**) and *Npc1*$^{-/-}$ (**H**) mouse brains. The lysosomal and cytosolic fractions were prepared using a lysosomal isolation kit. Note the relatively higher cytosolic levels of cathepsin D in the cerebellum compared with hippocampus. Cat B, cathepsin B; Cat D, cathepsin D; Cere, cerebellum; Cyto c, cytochrome *c*; CYTO, cytoplasmic; GAPDH, glyceraldehyde-3-phosphate dehydrogenase; Hippo, hippocampus; MB, membrane; NUC, nuclear, SKT, cytoskeletal.

age to mitochondria may cause release of other factors such as AIF, which can trigger cell death in a caspase-independent manner after its translocation to the nucleus.[58]

To establish the role of cathepsins in selective vulnerability of neurons in *Npc1*$^{-/-}$ mice, we first determined the subcellular (cytoskeletal, cytosolic, membrane, and nuclear) distribution of cathepsins B and D in the hippocampal, cortical, and cerebellar regions of 4-, 7-, and 10-week-old *Npc1*$^{-/-}$ and age-matched control mice. Our results revealed that cytosolic cathepsins B and D levels were markedly higher in the cerebellum and cortex than in the hippocampus of 4-, 7-, and 10-week-old *Npc1*$^{-/-}$ mice compared with controls (Figure 7, A–F, Supplemental Figure S2, see *http://ajp. amjpathol.org*; only 7-week data are shown). Within the cerebellum, the levels of the cytosolic cathepsins were relatively higher in all age groups but were more evident in 7- and 10-week-old *Npc1*$^{-/-}$ mice than in 4-week-old *Npc1*$^{-/-}$ mice. Similar to cathepsins, the levels of cytochrome *c* and Bax2, but not those of AIF, were increased predominantly in the cerebellar cytosolic fraction of 7- and 10-week-old *Npc1*$^{-/-}$ mice. In contrast to the cerebellum, we did not observe any drastic changes in the levels of cytochrome *c*, Bax2, or AIF in the hippocampus of *Npc1*$^{-/-}$ mice (Figure 7, A–D). To validate these results we fractionated lysosomal and cytosolic proteins from the hippocampus and cerebellum of 7-week-old *Npc1*$^{-/-}$ and control mice using the lysosomal isolation kit and then measured the levels of cathepsin D. Our results clearly showed that levels of cathepsin D were higher in the lysosomal fractions isolated from hippocampal and cerebellar regions of *Npc1*$^{-/-}$ mice compared with those of age-matched controls. Furthermore, the cytosolic levels of this enzyme were found to be markedly higher in the cerebellum than in the hippocampus of *Npc1*$^{-/-}$ mouse brains (Figure 7, G and H).

Lysosomal Enzymes and U18666A-Induced Loss of Cultured Neurons

Earlier studies have shown that the class 2 amphiphile U18666A can induce cell death by altering the trafficking

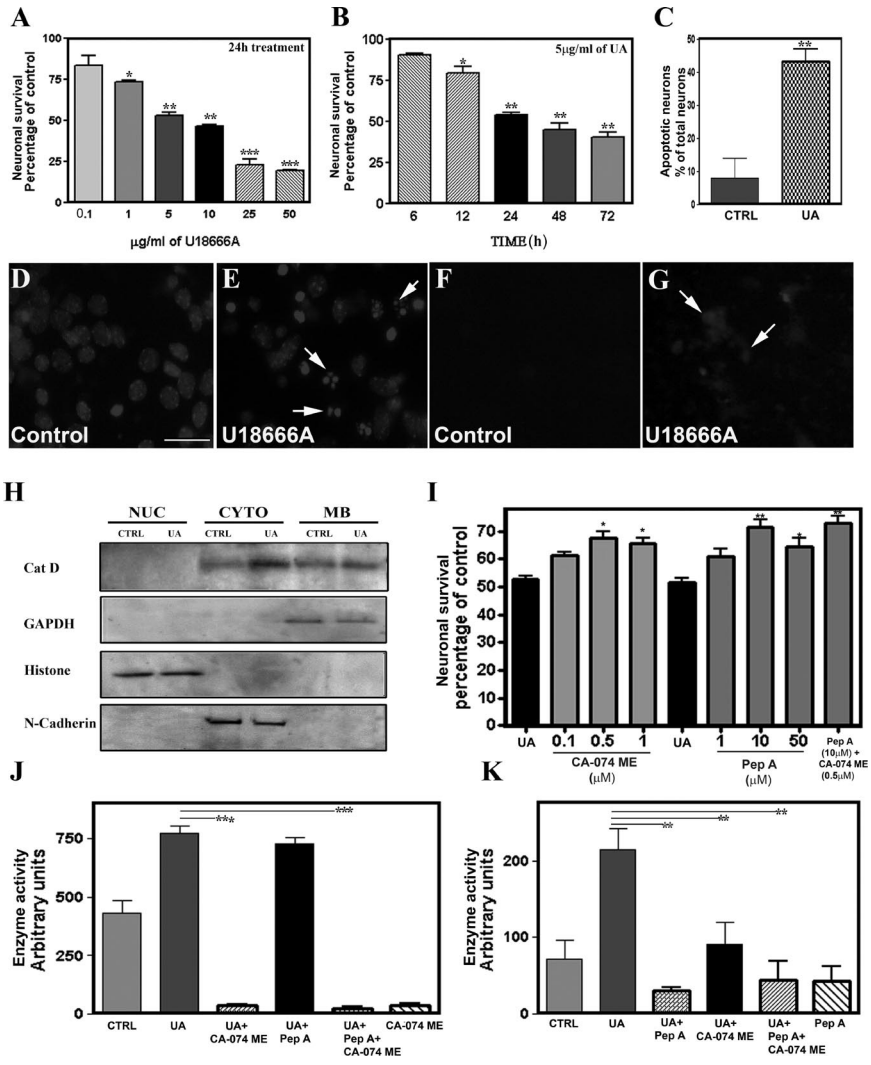

Figure 8. A–E: Neurotoxic effects of U18666A on mouse primary cortical cultured neurons as evident by MTT colorimetric assay (**A** and **B**) and Hoechst 33258 labeling (**C–E**). Neurons after 6 days of plating were treated with 0.1 to 50 μg/ml U18666A for 24 hours (**A**) or with 5 μg/ml U18666A for 6 to 72 hours (**B**). MTT values, as evident from the histograms, were significantly attenuated in a concentration- (**A**) and time (**B**)-dependent manner in U18666A-treated cultures. **C:** Relative increase in Hoechst 33258-labeled apoptotic neurons after 24 hours exposure to 5 μg/ml U18666A. **D** and **E:** Presence of condensed and/or fragmented nuclei (**arrows**) in U18666A-treated cultured neurons (**E**) compared with control (**D**). **F** and **G:** Cholesterol accumulation as evident by filipin staining in U18666A-treated cultured neurons (**G, arrows**) compared with control (**F**). **H:** Immunoblots showing the relatively higher cytosolic levels of cathepsin D in U18666A-treated cultured neurons compared with control cultures. **I:** Protective effects of the cathepsin B inhibitor CA-074 methyl ester and the cathepsin D inhibitor pepstatin A against U18666A-mediated toxicity in cortical cultured neurons as measured using the MTT assay. Note that both CA-074 methyl ester and pepstatin A can independently protect cultured neurons against 5 μg/ml U18666A-mediated toxicity, but their effects were not additive. **J** and **K:** Cathepsin B (**J**) and cathepsin D (**K**) enzyme activity in cultured neurons treated with 5 μg/ml U18666A either in the presence or absence of CA-074 methyl ester and pepstatin A. The increased enzyme activity observed after exposure to U18666A was significantly attenuated by treatment with CA-074 methyl ester as well as pepstatin A. Also note the attenuation of cathepsin D enzyme activity in cultured neurons treated with U18666A and CA-074 methyl ester. All results, which are presented as means ± SEM, were obtained from three separate experiments, each performed in triplicate. CA-074 ME, CA-074 methyl ester; Cat D, cathepsin D; CTRL, control; CYTO, cytoplasmic; GAPDH, glyceraldehyde-3-phosphate dehydrogenase; MB, membrane; Pep A, pepstatin A; NUC, nuclear; UA, U18666A. Scale bar = 25 μm. $^{*}P < 0.05$; $^{**}P < 0.01$; $^{***}P < 0.001$.

as well as the accumulation of cholesterol, thereby recapitulating the NPC1 phenotype.[53,59,60] We therefore used U18666A-induced toxicity in cultured mouse neurons from the cortex, an area known to be affected in NPC pathology, to determine the significance of cathepsins B and D in the degeneration of neurons in NPC disease (Figure 8, A–K). Our results showed that cultured mouse cortical neurons, which contain <10% glial cells (Supplemental Figure S3, see *http://ajp.amjpathol.org*) were vulnerable to U18666A-induced toxicity, as evident by a reduction in MTT values and the concurrent decrease in viable neurons after Hoechst 33258 nuclear staining (Figure 8, A–E). A concentration-dependent (0.1 to 50 μg/ml) effect of U18666A over a 24-hour treatment revealed a significant progressive decrease in MTT values from a dose of 1 μg/ml upward. Exposure of cultured neurons to 5 μg/ml U18666A decreased MTT values in a time-dependent (6 to 72 hours) manner, with a marked reduction in cell viability observed after 12 hours of treatment (Figure 8, A and B). The toxicity of U18666A on cortical cultured neurons was supported by an increased number of Hoechst 33258-positive apoptotic neurons (Figure 8, C–E). Accompanying the toxicity, filipin-labeled cholesterol was increased in cultured neurons after 24 hours of treatment with 5 μg/ml U18666A (Figure 8, F and G).

The activity of cathepsins B and D, as observed in NPC1 pathology, markedly increased after a 24-hour treatment of cultured neurons with U18666A (Figure 8, J and K). In addition, our subcellular studies revealed that the cytosolic levels of active cathepsins B and D were markedly higher in U18666A-treated neurons compared with untreated neurons (Figure 8H). Subsequently, to determine whether increased lysosomal enzyme activity was the cause or consequence of cell death, cultured neurons were treated with the cathepsin D inhibitor pepstatin A (1 to 50 μmol/L) or the cathepsin B inhibitor CA-074 methyl ester (0.05 to 1 μmol/L) for 24 hours along with 5 μg/ml U18666A, and then cell viability was assessed using the MTT assay (Figure 8I) and Hoechst 33258 staining (data not shown). The concentrations of cathepsin B and cathepsin D inhibitors used were based on earlier data.[61] Our results showed that both pepstatin A (10 and 20 μmol/L) and CA-074 methyl ester (0.5 and 1 μmol/L) can significantly protect cultured neurons against U18666A-induced toxicity and were effective in inhibiting their corresponding enzyme activity (Figure 8,I–

K). In addition, treatments with pepstatin A and CA-074 methyl ester together protected cultured neurons against U18666A-mediated toxicity to a similar extent as observed after treatment with either inhibitor alone (Figure 8I).

Discussion

Using a combination of experimental approaches, in the present study we show that increased levels/activity of cathepsins B and D may be associated with neuronal loss observed in *Npc1*$^{-/-}$ mouse brains. Our results reveal that i) *Npc1*$^{-/-}$ mice exhibit an age-dependent loss of neurons primarily in the cerebellum and not in the hippocampal region of the brain, ii) cellular levels and activity of cathepsins B and D are increased in both the cerebellum and hippocampus of *Npc1*$^{-/-}$ mouse brains most likely because of microgliosis, but cytosolic cathepsin B and D levels and other indices of cell death are found to be different between these two brain regions, and iii) degeneration of cultured mouse cortical neurons by U18666A, an amphiphilic drug that induces a NPC-like phenotype at the cellular level, can be significantly attenuated through inhibition of cathepsin activity. Taken together, these results suggest that increased activity, along with increased cytosolic levels, of cathepsins B and D may be associated with the degeneration of NPC1-deficient neurons and inhibitors of these enzymes might protect neurons in *Npc1*$^{-/-}$ mouse brains.

Earlier studies have shown that severe loss of neurons/terminals in *Npc1*$^{-/-}$ mice is evident largely in the cerebellar Purkinje cells, whereas hippocampal neurons are relatively spared.[13–15,18] At present, the cell death mechanism remains unclear as events related to both apoptosis and autophagy have been identified in *Npc1*$^{-/-}$ mouse brains. Detection of terminal deoxynucleotidyl transferase dUTP nick-end labeling-positive and active caspase-3-immunoreactive Purkinje cells[62,63] is consistent with cell death being due to apoptosis. In keeping with these results, we observed cleaved caspase-3 and Fluoro-Jade C-positive Purkinje cells in the cerebellum but not in the hippocampus of *Npc1*$^{-/-}$ mice. However, antiapoptotic strategies, such as overexpression of Bcl-2 or treatment with minocycline, that are known to prevent apoptosis in some models of neurodegenerative diseases failed to protect neurons in *Npc1*$^{-/-}$ mice,[64] suggesting the possible existence of redundant apoptotic mechanisms in NPC pathology. Interestingly, our results revealed that the numbers of secondary lysosomes as well as of the autophagy markers LC3-II and beclin-1 are higher in both the cerebellum and hippocampus of *Npc1*$^{-/-}$ mice compared with controls as reported in earlier studies.[49,50] Because autophagy can be induced during both survival and death of cells,[9,65] the significance of the enhanced autophagic pathway in *Npc1*$^{-/-}$ mice remains to be defined.

Although the intracellular accumulation of unesterified cholesterol per se does not correlate directly with the degeneration of neurons, there is evidence that an increased cholesterol level in the EL system can up-regulate lysosomal enzymes within cells.[21,49,66] This finding is substantiated, in part, by our study, which shows an age-related increase in the expression, level, and activity of the lysosomal enzymes, cathepsins B and D, both in the hippocampus and cerebellum of *Npc1*$^{-/-}$ mice compared with controls. Double immunofluorescence analysis further revealed that cathepsins B and D are present both in neurons and activated microglia in the hippocampus and cerebellum of *Npc1*$^{-/-}$ mice.[16,49] Earlier studies indicated that an increased level of lysosomal enzymes within lysosomes might be involved in protecting neurons against toxicity/damage, whereas increased activity of these enzymes in cell cytosol can trigger death of neurons.[20,32,51,52] However, it remains unclear whether increased levels/activity of the lysosomal enzymes observed in *Npc1*$^{-/-}$ mouse brains are involved in the protection or degeneration of neurons. Our subcellular localization studies showed for the first time that cytosolic levels of cathepsins B and D are markedly increased in the cerebellum, but are only slightly increased in the relatively spared hippocampus of *Npc1*$^{-/-}$ mice. It is thus likely that enhanced levels of lysosomal enzymes in the hippocampus may counter cellular abnormalities resulting from intracellular cholesterol accumulation and may not reach levels necessary to mediate cell death. On the other hand, larger increases in cytosolic levels of the cathepsins in the cerebellum, probably resulting from lysosomal destabilization, may be associated with death of neurons via cytochrome *c* release from mitochondria. This suggestion is supported by evidence that cytosolic levels of cytochrome c and Bax2 in *Npc1*$^{-/-}$ mice are increased mostly in the cerebellum but not in the hippocampus. The significance of cathepsins is further substantiated by evidence that degeneration of cultured cortical neurons by U18666A, which induces cholesterol accumulation in the EL system similar to NPC1 deficiency,[53,60] is accompanied by increased activity of these enzymes and can be significantly attenuated after treatment with inhibitors of cathepsin B or cathepsin D. However, exposure of cultured neurons to inhibitors of cathepsins B and D together did not produce additive effects on the survival of neurons. This result could be due to either the effects of cathepsin D inhibitor on cathepsin B enzyme activity or the use of a common mechanism to mediate the effects. Taken together, these results suggest that increased cathepsin levels/activity may be associated with the loss of Purkinje cells in *Npc1*$^{-/-}$ mice and their inhibitors may be beneficial in protecting these neurons.

We did not observe any significant alteration in IGF-II/M6P receptor levels in the hippocampus or cerebellum of *Npc1*$^{-/-}$ mice compared with controls. Given the evidence that a subset of reactive astrocytes in *Npc1*$^{-/-}$ mouse brains express the IGF-II/M6P receptor, it is likely that decreased neuronal levels of the receptor are partially compensated for by glial expression of the receptor. Interestingly, activated microglia that exhibit cathepsin B and D immunoreactivity did not express IGF-II/M6P receptors in *Npc1*$^{-/-}$ mouse brains. This observation is consistent with some earlier results that showed a disparity in the localization of the lysosomal enzymes and the receptor in glial cells after injury or pathological condi-

tions.[16,33,46,67,68] Because certain lysosomal enzymes can be transported via a cation-dependent M6P receptor in selected cells,[22,69] it is possible that cathepsins in reactive microglia may be transported by a cation-dependent M6P receptor rather than the IGF-II/M6P receptor. Earlier studies using cultured cells have shown that U18666A treatment or siRNA-mediated NPC1 depletion, can redistribute IGF-II/M6P receptors to cholesterol-laden endosomes and impair receptor recycling from late endosomes to the *trans*-Golgi network.[70–72] Although the subcellular distribution of the receptor in *Npc1*$^{-/-}$ mouse brains remains to be defined, an altered distribution or decreased levels of the M6P receptors might render neurons vulnerable to dysfunction/degeneration by enhancing the secretion of lysosomal enzymes. This idea is supported, in part, by the evidence that suppression of the IGF-II/M6P receptor can induce apoptosis,[73] whereas cells resistant to toxicity/injury exhibit an up-regulation of the receptor.[33,74]

A number of previous studies have shown that dysfunction of the NPC1 protein leads to degeneration of neurons in selected regions of the brain including the cerebellum, cortex, thalamus, and brainstem.[13–15,18] However, neither the intracellular mechanisms nor the underlying cause of preferential vulnerability of these neurons has been established. Some recent studies have indicated that deregulation of the phosphatidylinositol-3 kinase pathway[75] and/or β-amyloid peptide-mediated signaling cascades[21,66,76] may contribute to the degeneration of neurons in *Npc1*$^{-/-}$ mouse brains. However, the significance of these pathways in defining the underlying cause of preferential neuronal vulnerability in *Npc1*$^{-/-}$ mouse brains remains unclear. Our results, on the other hand, show that increased levels/activity of the lysosomal enzymes cathepsins B and D, possibly within lysosomes, may protect neurons against toxicity induced by intracellular accumulation of cholesterol, whereas increased cytosolic levels/activity of cathepsins may render neurons vulnerable to degeneration via a cytochrome *c*-dependent pathway. The significance of the lysosomal enzymes is highlighted by the fact that inhibitors of these enzymes can protect cultured neurons against U18666A-mediated toxicity. Thus, these results provide the first evidence that the increased level/activity as well as altered subcellular distribution of cathepsins B and D may contribute to the neurodegeneration seen in NPC disease. Furthermore, inhibitors of the cathepsins may have therapeutic potential in attenuating NPC pathology.

References

1. Carstea ED, Morris JA, Coleman KG, Loftus SK, Zhang D, Cummings C, Gu J, Rosenfeld MA, Pavan WJ, Krizman DB, Nagle J, Polymeropoulos MH, Sturley SL, Ioannou YA, Higgins ME, Comly M, Cooney A, Brown A, Kaneski CR, Blanchette-Mackie EJ, Dwyer NK, Neufeld EB, Chang TY, Liscum L, Strauss JF 3rd, Ohno K, Zeigler M, Carmi R, Sokol J, Markie D, O'Neill RR, van Diggelen OP, Elleder M, Patterson M, Brady RO, Vanier MT, Pentchev PG, Tagle DA: Niemann-Pick C1 disease gene: homology to mediators of cholesterol homeostasis. Science 1997, 277:228–231
2. Naureckiene S, Sleat DE, Lackland H, Fensom A, Vanier MT, Wattiaux R, Jadot M, Lobel P: Identification of HE1 as the second gene of Niemann-Pick C disease. Science 2000, 290:2298–2301
3. Vanier MT, Millat G: Niemann-Pick disease type C. Clin Genet 2003, 64:269–281
4. Walkley SU, Suzuki K: Consequences of NPC1 and NPC2 loss of function in mammalian neurons. Biochim Biophys Acta 2004, 1685:48–62
5. Pentchev PV, Vanier MT, Suzuki K, Patterson MC: Niemann-Pick disease type C: a cellular cholesterol lipidosis. The Metabolic and Molecular Basis of Inherited Disease, vol II. Edited by CR Scriver, AL Beaudet, WD Sly, D Valle. New York, McGraw-Hill, 1995, pp 2625–2639
6. Vanier MT, Suzuki K: Recent advances in elucidating Niemann-Pick C disease. Brain Pathol 1998, 8:163–174
7. Mukherjee S, Maxfield FR: Lipid and cholesterol trafficking in NPC. Biochim Biophys Acta 2004, 1685:28–37
8. Vance JE: Lipid imbalance in the neurological disorder, Niemann-Pick C disease. FEBS Lett 2006, 580:5518–5524
9. Pacheco CD, Lieberman AP: The pathogenesis of Niemann-Pick type C disease: a role for autophagy ? Expert Rev Mol Med 2008, 10:e26
10. Loftus SK, Morris JA, Carstea ED, Gu JZ, Cummings C, Brown A, Ellison J, Ohno K, Rosenfeld MA, Tagle DA, Pentchev PG, Pavan WJ: Murine model of Niemann-Pick C disease: mutation in a cholesterol homeostasis gene. Science 1997, 277:232–235
11. Karten B, Vance DE, Campenot RB, Vance JE: Trafficking of cholesterol from cell bodies to distal axons in Niemann Pick C1 deficient neurons. J Biol Chem 2003, 278:4168–4175
12. Paul CA, Boegle AK, Maue RA: Before the loss: neuronal dysfunction in Niemann-Pick type C disease. Biochim Biophys Acta 2004, 1685:63–76
13. Li H, Repa JJ, Valasek MA, Beltroy EP, Turley SD, German DC, Dietschy JM: Molecular, anatomical, and biochemical events associated with neurodegeneration in mice with Niemann-Pick type C disease. J Neuropathol Exp Neurol 2005, 64:323–333
14. Ong WY, Kumar U, Switzer RC, Sidhu A, Suresh G, Hu CY, Patel SC: Neurodegeneration in Niemann-Pick type C disease mice. Exp Brain Res 2001, 141:218–231
15. German DC, Quintero EM, Liang CL, Ng B, Punia S, Xie C, Dietschy JM: Selective neurodegeneration, without neurofibrillary tangles, in a mouse model of Niemann-Pick C disease. J Comp Neurol 2001, 433:415–425
16. German DC, Liang CL, Song T, Yazdani U, Xie C, Dietschy JM: Neurodegeneration in the Niemann-Pick C mouse: glial involvement. Neuroscience 2002, 109:437–450
17. Baudry M, Yao Y, Simmons D, Liu J, Bi X: Postnatal development of inflammation in a murine model of Niemann-Pick type C disease: immunohistochemical observations of microglia and astroglia. Exp Neurol 2003, 184:887–903
18. Sarna JR, Larouche M, Marzban H, Sillitoe RV, Rancourt DE, Hawkes R: Patterned Purkinje cell degeneration in mouse models of Niemann-Pick type C disease. J Comp Neurol 2003, 456:279–291
19. Bahr BA, Bendiske J: The neuropathogenic contributions of lysosomal dysfunction. J Neurochem 2002, 83:481–489
20. Turk B, Stoka V, Rozman-Pungercar J, Cirman T, Droga-Mazovec G, Oresic K, Turk V: Apoptotic pathways: involvement of lysosomal proteases. Biol Chem 2002, 383:1035–1044
21. Nixon RA, Yang DS, Lee JH: Neurodegenerative lysosomal disorders: a continuum from development to late age. Autophagy 2008, 4:590–599
22. Dahms NM, Hancock MK: P-type lectins. Biochim Biophys Acta 2002, 1572:317–340
23. Ghosh P, Dahms NM, Kornfeld S: Mannose 6-phosphate receptors: new twists in the tale. Nat Rev Mol Cell Biol 2003, 4:202–212
24. Hawkes C, Kar S: The insulin-like growth factor-II/mannose-6-phosphate receptor: structure, distribution and function in the central nervous system. Brain Res Rev 2004, 44:117–140
25. Nixon RA, Mathews PM, Cataldo AM: The neuronal endosomal-lysosomal system in Alzheimer's disease. J Alzheimers Dis 2001, 3:97–107
26. Wraith JE: Lysosomal disorders. Semin Neonatol 2002, 7:75–83
27. Tardy C, Andrieu-Abadie N, Salvayre R, Levade T: Lysosomal storage diseases: is impaired apoptosis a pathogenic mechanism? Neurochem Res 2004, 29:871–880
28. Roberg K, Ollinger K: Oxidative stress causes relocation of the lysosomal enzyme cathepsin D with ensuing apoptosis in neonatal rat cardiomyocytes. Am J Pathol 1998, 152:1151–1156
29. Yamashima T, Kohda Y, Tsuchiya K, Ueno T, Yamashita J, Yoshioka

T, Kominami E: Inhibition of ischemic hippocampal neuronal death in primates with cathepsin B inhibitor CA-074: a novel strategy for neuroprotection based on 'calpain-cathepsin hypothesis.' Eur J Neurosci 1998, 10:1723–1733
30. Yong AP, Bednarski E, Gall CM, Lynch G, Ribak CE: Lysosomal dysfunction results in lamina-specific maganeurite formation but not apoptosis in frontal cortex. Exp Neurol 1999, 157:150–160
31. Barlow C, Ribaut-Barassin C, Zwingman TA, Pope AJ, Brown KD, Owens JW, Larson D, Harrington EA, Haeberle AM, Mariani J, Eckhaus M, Herrup K, Bailly Y, Wynshaw-Boris A: ATM is a cytoplasmic protein in mouse brain required to prevent lysosomal activation. Proc Natl Acad Sci USA 2000, 97:871–876
32. Bendiske J, Bahr BA: Lysosomal activation is a compensatory response against protein accumulation and associated synaptogenesis-an approach for slowing Alzheimer disease? J Neuropathol Exp Neurol 2003, 62:451–463
33. Hawkes C, Kabogo D, Amritraj A, Kar S: Up-regulation of cation-independent mannose 6-phosphate receptor and endosomal–lysosomal markers in surviving neurons following 192 IgG-saporin administrations into the adult rat brain. Am J Pathol 2006, 169:1140–1154
34. MacDonald RG, Tepper MA, Clairmont KB, Perregaux SB, Czech MP: Serum form of the rat insulin-like growth factor II/mannose 6-phosphate receptor is truncated in the carboxyl-terminal domain. J Biol Chem 1989, 264:3256–3261
35. O'Gorman DB, Weiss J, Hettiaratchi A, Firth SM, Scott CD: Insulin-like growth factor-II/mannose 6-phosphate receptor overexpression reduces growth of choriocarcinoma cells in vitro and in vivo. Endocrinology 2002, 143:4287–4294
36. Song MS, Rauw G, Baker GB, Kar S: Memantine protects rat cortical cultured neurons against β-amyloid-induced toxicity by attenuating tau phosphorylation. Eur J Neurosci 2008, 28:1989–2002
37. Zheng WH, Bastianetto S, Mennicken F, Ma W, Kar S: Amyloid β peptide induces tau phosphorylation and neuronal degeneration in rat primary septal cultured neurons. Neuroscience 2002, 115:201–211
38. Wei Z, Song MS, MacTavish D, Jhamandas JH, Kar S: Involvement of calpain and caspase in β-amyloid-induced cell death in rat primary septal cultured neurons. Neuropharmacology 2008, 54:721–733
39. Myher JJ, Kuksis A, Pind S: Molecular species of glycerophospholipids and sphingomyelins of human plasma: comparison to red blood cells. Lipids 1989, 24:408–418
40. Jacobs RL, Lingrell S, Zhao Y, Francis GA, Vance DE: Hepatic CTP:phosphocholine cytidylytransferase-α is a critical predictor of plasma high density lipoprotein and very low density lipoprotein. J Biol Chem 2008, 283:2147–2155
41. Bornig H, Geyer G: Staining of cholesterol with the fluorescent antibiotic "filipin." Acta Histochem 1974, 50:110–115
42. Schmued LC, Stowers CC, Scallet AC, Xu L: Fluoro-Jade C results in ultra high resolution and contrast labeling of degenerating neurons. Brain Res 2005, 1035:24–31
43. Salio C, Lossi L, Ferrini F, Merighi A: Ultrastructural evidence for a pre- and postsynaptic localization of full-length trkB receptors in substantia gelatinosa (lamina II) of rat and mouse spinal cord. Eur J Neurosci 2005, 8:1951–1966
44. Hawkes C, Jhamandas JH, Harris K, Fu J, MacDonald RG, Kar S: Single transmembrane IGF-II/M6P receptor regulates central cholinergic function by activating a G protein-sensitive, protein kinase C-dependent pathway. J Neurosci 2006, 26:585–596
45. Jafferali S, Dumont Y, Sotty F, Robitaille Y, Quirion R, Kar S: Insulin-like growth factor-I and its receptor in the frontal cortex, hippocampus and cerebellum of normal human and Alzheimer's disease brains. Synapse 2000, 38:450–459
46. Amritraj A, Hawkes C, Phinney AL, Mount TH, Scott CD, Westaway D, Kar S: Altered levels and distribution of IGF-II/M6P receptor and lysosomal enzymes in mutant APP and APP + PS1 transgenic mouse brains. Neurobiol Aging 2009, 30:54–70
47. Karten B, Vance DE, Campenot RB, Vance JE: Cholesterol accumulates in cell bodies, but is decreased in distal axons, of Niemann-Pick C1-deficient neurons. J Neurochem 2002, 83:1154–1163
48. Mariño G, Lopez-Otin C: Autophagy: molecular mechanisms, physiological functions and relevance in human pathology. Cell Mol Life Sci 2004, 61:1439–1454
49. Liao G, Yao Y, Liu J, Yu Z, Cheung S, Xie A, Liang X, Bi X: Cholesterol accumulation is associated with lysosomal dysfunction and autophagic stress in Npc1$^{-/-}$ mouse brain. Am J Pathol 2007, 171:962–975
50. Pacheco CD, Kunkel R, Lieberman AP: Autophagy in Niemann-Pick C disease is dependent upon beclin-1 and responsive to lipid trafficking defects. Hum Mol Genet 2007, 16:1495–1503
51. Bursch W: The autophagosomal-lysosomal compartment in programmed cell death. Cell Death Differ 2001, 8:569–581
52. Chwieralski C, Welte T, Buhling F: Cathepsin-regulated apoptosis. Apoptosis 2006, 11:143–149
53. Cheung NS, Koh CH, Bay BH, Qi RZ, Choy MS, Li QT, Wong KP, Whiteman M: Chronic exposure to U18666A induces apoptosis in cultured murine cortical neurons. Biochem Biophys Res Commun 2004, 315:408–417
54. Oberst A, Bender C, Green DR: Living with death: the evolution of the mitochondrial pathway of apoptosis in animals. Cell Death Differ 2008, 7:1139–1146
55. Zhao M, Antunes F, Eaton JW, Brunk UT: Lysosomal enzymes promote mitochondrial oxidant production, cytochrome *c* release and apoptosis. Eur J Biochem 2003, 270:3778–3786
56. Heinrich M, Neumeyer J, Jakob M, Hallas C, Tchikov V, Winoto-Morbach S, Wickel M, Schneider-Brachert W, Trauzoid A, Hethke A, Schutze S: Cathespin D links TNF-induced acid sphingomyelinase to Bid-mediated caspase-9 and -3 activation. Cell Death Differ 2004, 11:550–563
57. Droga-Mazovec G, Bojic L, Petelin A, Ivanova S, Romih R, Repnik U, Salvesen GS, Stoka V, Turk V, Turk B: Cysteine cathepsins trigger caspase-dependent cell death through cleavage of bid and antiapoptotic Bcl-2 homologues. J Biol Chem 2008, 283:19140–19150
58. Candé C, Vahsen N, Garrido C, Kroemer G: Apoptosis-inducing factor (AIF): caspase-independent after all. Cell Death Differ 2004, 11:591–595
59. Huang Z, Hou Q, Cheung NS, Li QT: Neuronal cell death caused by inhibition of intracellular cholesterol trafficking is caspase dependent and associated with activation of the mitochondrial apoptosis pathway. J Neurochem 2006, 97:280–291
60. Koh CH, Whiteman M, Li QX, Halliwell B, Jenner AM, Wong BS, Laughton KM, Wenk M, Masters CL, Beart PM, Bernard O, Cheung NS: Chronic exposure to U18666A is associated with oxidative stress in cultured murine cortical neurons. J Neurochem 2006, 98:1278–1289
61. Figueiredo C, Pais TF, Gomes JR, Chatterjee S: Neuron-microglia crosstalk up-regulates neuronal FGF-2 expression which mediates neuroprotection against excitotoxicity via JNK1/2. J Neurochem 2008, 107:73–85
62. Wu YP, Mizukami H, Matsuda J, Saito Y, Proia R, Suzuki K: Apoptosis accompanied by up-regulation of TNF-α death pathway genes in the brain of Niemann-Pick type C disease. Mol Genet Metab 2005, 84:9–17
63. Alvarez AR, Klein A, Castro J, Cancino GI, Amigo J, Mosqueira M, Vargas LM, Yévenes LF, Bronfman FC, Zanlungo S: Imatinib therapy blocks cerebellar apoptosis an improves neurological symptoms in a mouse model of Niemann-Pick type C disease. FASEB J 2008, 10:3617–3627
64. Erickson RP, Bernard O: Studies on neuronal death in the mouse model of Niemann-Pick C disease. J Neurosci Res 2002, 68:738–744
65. Butler D, Brown QB, Chin DJ, Batey L, Karim S, Mutneja MS, Karanian DA, Bahr BA: Cellular responses to protein accumulation involve autophagy and lysosomal enzyme activation. Rejuvenation Res 2005, 8:227–231
66. Jin L, Maezawa I, Vincent I, Bird T: Intracellular accumulation of amyloidogenic fragments of amyloid-β precursor protein in neurons with Niemann-Pick type C defects is associated with endosomal abnormalities. Am J Pathol 2004, 164:975–985
67. Dagvajantsan B, Aoki M, Warita H, Suzuki N, Itoyama Y: Up-regulation of insulin-like growth factor-II receptor in reactive astrocytes in the spinal cord of amyotrophic lateral sclerosis transgenic rats. Tohoku J Exp Med 2008, 214:303–310
68. Nakanishi H: Neuronal and microglial cathepsins in aging and age-related diseases. Ageing Res Rev 2003, 2:367–381
69. Sleat DE, Lobel P: Ligand binding specificities of the two mannose 6-phosphate receptors. J Biol Chem 1997, 272:731–738
70. Kobayashi T, Beuchat MH, Lindsay M, Frias S, Palmiter RD, Sakuraba H, Parton RG, Gruenberg J: Late endosomal membranes rich in lysobisphosphatidic acid regulate cholesterol transport. Nat Cell Biol 1999, 1:113–118
71. Ganley IG, Pfeffer SR: Cholesterol accumulation sequesters Rab9

and disrupts late endosome function in NPC1-deficient cells. J Biol Chem 2006, 281:17890–17899
72. Ikeda K, Hirayama M, Hirota Y, Asa E, Seki J, Tanaka J: Drug-induced phospholipidosis is caused by blockade of mannose 6-phosphate receptor-mediated targeting of lysosomal enzymes. Biochem Biophys Res Commun 2008, 377:268–274
73. Zhou G, Roizman B: Cation-independent mannose 6-phosphate receptor blocks apoptosis induced by herpes simplex virus 1 mutants lacking glycoprotein D and is likely the target of antiapoptotic activity of the glycoprotein. J Virol 2002, 76:6197–6204
74. Li Y, Xu C, Schubert D: The up-regulation of endosomal-lysosomal components in amyloid beta-resistant cells. J Neurochem 1999, 73:1477–1482
75. Bi X, Liu J, Yao Y, Baudry M, Lynch G: Deregulation of the phosphatidylinositol-3 kinase signaling cascade is associated with neurodegeneration in Npc1$^{-/-}$ mouse brain. Am J Pathol 2005, 67:1081–1092
76. Burns M, Gaynor K, Olm V, Mercken M, LaFrancois J, Wang L, Mathews PM, Noble W, Matsuoka Y, Duff K: Presenilin redistribution associated with aberrant cholesterol transport enhances β-amyloid production in vivo. J Neurosci 2003, 23:5645–5649